FUNCTIONAL SILVER NANOWIRES

A THESIS SUBMITTED TO

THE GRADUATE SCHOOL OF NATURAL AND APPLIED SCIENCES

OF

MIDDLE EAST TECHNICAL UNIVERSITY

BY

ECE ALPUĞAN

IN PARTIAL FULLFILLMENT OF THE REQUIREMENTS

FOR

THE DEGREE OF MASTER OF SCIENCE

IN

METALLURGICAL AND MATERIALS ENGINEERING

JANUARY 2018

Approval of the thesis:

FUNCTIONAL SILVER NANOWIRES

submitted by **ECE ALPUĞAN** in partial fulfillment of the requirements for the degree of **Master of Science in Metallurgical and Materials Engineering Department, Middle East Technical University** by,

Prof. Dr. Halil Kalıpçılar   _____
Dean, Graduate School of **Natural and Applied Sciences**

Prof. Dr. C.Hakan Gür   _____
Head of Department, **Metallurgical and Mat. Eng. Dept., METU**

Assoc. Prof. Dr. H. Emrah Ünalan   _____
Supervisor, **Metallurgical and Materials Eng. Dept., METU**

Prof. Dr. F.Arcan Dericioğlu   _____
Co-Supervisor, **Metallurgical and Materials Eng. Dept., METU**

Examining Committee Members:

Prof. Dr. Özlem Aydın Çivi   _____
Electric and Electronic Engineering Dept., METU

Assoc. Prof. Dr. H. Emrah Ünalan   _____
Metallurgical and Materials Engineering Dept., METU

Prof. Dr. Arcan F. Dericioğlu   _____
Metallurgical and Materials Engineering Dept., METU

Assoc. Prof. Dr. Görkem Günbaş   _____
Chemistry Dept., METU

Assoc. Prof. Dr. Ziya Esen   _____
Materials Science and Eng. Dept.,Çankaya University

Date: 31.01.2018

I hereby declare that all information in this document has been obtained and presented in accordance with academic rules and ethical conduct. I also declare that, as required by these rules and conduct, I have fully cited and referenced all material and results that are not original to this work.

Name, Last name: Ece Alpuğan

Signature:

ABSTRACT

FUNCTIONAL SILVER NANOWIRES

Alpuğan, Ece

M.S., Department of Metallurgical and Materials Engineering

Supervisor: Assoc. Prof. Dr. H. Emrah Ünalan

Co-Supervisor: Prof. Dr. Arcan F. Dericioğlu

January 2018, 87 pages

Silver nanowires (Ag NWs) are one of the most promising nanomaterials for future optoelectronic devices. They have high thermal and electrical conductivity and high transparency in network form, which are the key properties for various applications. The use of Ag NWs have been demonstrated in heaters, photodetectors and biosensors. In this thesis, firstly, Ag NW networks are used as electromagnetic interference shields on different substrates such as polyethylene terephthalate (PET), textile, filter paper and felt. Ag NWs are spray coated onto PET substrates, while dip coating method is used for filter paper, textiles and felt substrates. Maximum shielding is obtained with the Ag NW coated filter paper sample with a resistance of 10 ohm. Almost 99 % shielding is observed. Secondly, Ag NWs are used as top and bottom electrodes for organic solar cells. For bottom electrodes, Ag NWs are spray coated onto glass substrates. The device structure for these solar cells is Ag NW/PEDOT: PSS/P3HT: PCBM/ LiF /Al. A control sample was fabricated on commercially available indium tin oxide (ITO) thin films. A power conversion efficiency of 1.13 % is obtained from

solar cells with Ag NW bottom electrodes, while a conversion efficiency of 3.15 % is obtained from ITO control sample. For top electrodes in inverted solar cell structure, Ag NWs on polydimethylsiloxane (PDMS) substrates are used and simply placed onto fabricated devices. The device structure for these solar cells is ITO/ZnO/P3HT:PCBM/PEDOT:PSS/Ag NW-PDMS. A control device with gold top electrode is also fabricated. A power conversion efficiency of 1.73 % is obtained for top electrode devices, while that for the control device is 2.62 %. It is worth mentioning that these top electrode devices are partially transparent. All in all, very promising characteristics are obtained using Ag NWs both in electromagnetic interference shields and in organic solar cells as electrodes.

Keywords: silver nanowires, electromagnetic shielding, organic solar cells

ÖZ

FONKSİYONEL GÜMÜŞ NANOTELLER

Alpuğan, Ece

Yüksek Lisans, Metalurji ve Malzeme Mühendisliği Bölümü

Tez Danışmanı : Doç. Dr. H. Emrah Ünalan

Ortak Tez Danışmanı : Prof. Dr. Arcan Dericioğlu

Ocak 2018, 87 sayfa

Gümüş nanoteller gelecekteki optoelektronik cihaz uygulamalarında gelecek vaat eden nanomalzemelerden biridir. Yüksek ısı ve elektrik iletkenliği ve yüksek transparanlık gibi çoğu uygulamadaki anahtar özelliğe sahiptir. Isıtıcılarda, fotodetektörlerde ve biyosensörlerde kullanılmaktadır. Bu tezde, ilk olarak sentezlenen gümüş nanoteller elektromanyetik kalkan olarak poliethilen terephthalat, filtre kağıdı, kumaş ve keçe gibi farklı altlıklar üzerinde kullanılmıştır. Gümüş nanoteller PET atlığının üzerine spreyle kaplanırken, filter kağıdı, kumaş ve keçe üzerine daldırmalı kaplama method kullanılarak kaplanmıştır. Maksimum kalkanlama 10 ohm dirence sahip olan gümüş nanotel kaplanmıs olan filtre kağıdından elde edilmiştir. Yaklaşık % 99 kalkanlama gözlemlenmiştir. İkinci olarak, gümüş nanoteller organik güneş gözelerinde üst ve alt elektrot olarak kullanılmıştır.Alt elektrot olarak kullanılması için gümüş nanoteller sprey kaplama ile cama kaplanmıştır. Bu güneş gözesi için cihaz mimarisi Gümüş Nanotel /PEDOT:PSS/P3HT:PCBM/ LiF /Al şeklindedir. Kontrol numunesi ise piyasada satılan indiyum kalay oksit (ITO) ince filmlerle üretilmiştir. Gümüş nanotellerin alt elektrot olarak kullanıldığı güneş pilinden yüzde 1.13 güç dönüşüm verimi elde edilirken, ITO kullanılarak yapılan kontrol numunesinden yüzde 3.15 güç

dönüşümü elde edimiştir. Üst elektrot olarak ters güneş pillerinde kullanılırken, gümüş nanoteller PDMS kullanılarak transfer edilmiştir. Bu güneş pilleri için cihaz yapısı ITO/ZnO/P3HT:PCBM/PEDOT:PSS/Ag NW-PDMS şeklindedir. Üst elektrot olarak altın kullarak kontrol numunesi üretilmiştir. Gümüş nanotellerin üst elektrot olarak kullanıldığı güneş pilinden yüzde 1.73 güç dönüşüm verimi elde edilirken, altın kullanılarak yapılan kontrol numunesinden yüzde 2.62 güç dönüşümü elde edimiştir. Üst elektrotlu cihazların kısmen transparan olduğunu belirtmek gerekmektedir. Sonuç olarak, gümüş nanotelleri hem elektromanyetik girişim kalkanlama hem de organik güneş pillerinde elektrot olarak kullanarak umut vaad eden özellikler elde edilmiştir.

Anahtar Kelimeler: Gümüş nanoteller, elektromanyetik kalkanlama, organik güneş gözesi

To gorgeous people who raised me,

To my mother, my father and my grandmother,

To my family and my dear friends…

ACKNOWLEDGEMENTS

TABLE OF CONTENTS

LIST OF TABLES

TABLES

LIST OF FIGURES

FIGURES

CHAPTER 1

INTRODUCTION

Materials with high conductivity and high transparency received significant attention for the development of novel optoelectronic devices. One of the most commonly used nanomaterial for such purpose is silver nanowires (Ag NWs). Compared to thin film metals, similar conductivity values can be obtained through the use of silver nanowire networks even though less material is used. Two dimensional conductivity is maintained through the use of one dimensional silver nanowires, based on the percolation model. Essam et al. described this model as a collection of points distributed in space, certain pairs which are said to be adjacent or linked [1]. By this concept, concentration dependent insulator to conductor transition of conductive fillers within an insulator matrix is described [2]. To illustrate, Ag NWs are used as conductive fillers and coated onto insulator substrates. During coating up to a certain value of Ag NW density no conductivity is measured. After a critical density, which is called as percolation threshold, conductivity is measured and a suitable path for charge transport is formed. In addition, these Ag NW networks provide optical transparency. Their utilization has already been demonstrated in many applications including light emitting diodes (LED), transparent heaters, touch panels and sensors.

Coskun et al. replaced indium tin oxide (ITO) thin films with Ag NW networks in light emitting diodes [3]. Biggest challenge for the nanowire network is the higher surface roughness compared to that of ITO. This problem is solved through the use of a polymeric over layer. While the as deposited nanowire networks have a surface roughness of 54 nm, it is lowered to 5 nm with this over layer. A lower threshold voltage was obtained for the devices with Ag NW networks compared to those fabricated with commercially available ITO films.

ITO is also used for transparent heaters. However, there are some problems such as expensive vacuum based deposition for high quality ITO thin films, instable price of ITO due to indium and insufficient mechanical properties due to its crystalline nature. Therefore, alternative materials are highly sought to replace ITO. Ergun et al. used Ag NWs for the production of transparent heaters [4]. In this work, Ag NWs are spray coated over quartz substrates. A maximum bias of 5 V is applied to the network through two parallel contacts placed 2 cm apart and the heater reached up to 275°C. Flexible heaters are also demonstrated in this work.

Most of the technological devices now, have touch screens such as smartphones, game consoles, tablets and personal computers. The light emitted from the device goes through the front electrode. Therefore, the front electrode should have high transparency. Madaria et al. obtained highly uniform and large scale Ag NW networks through spray coating [5]. Fabricated networks have an optical transmittance of 85 % at a wavelength of 550 nm and a sheet resistance of 33 ohm/square, both of which are comparable to the ITO thin films used in touch panels nowadays.

Smart textiles recently started to appear in the market. As an example, strain sensors are placed over the cloths for the detection of human motion. Flexible and stretchable sensors are highly desired for this application. Amjadi et al. used sandwich structure composed of Ag NWs and polydimethylsiloxane (PDMS) for this purpose [6]. They obtain 70 % stretchability, which is much higher than the conventional strain sensors. A smart glove is also demonstrated within the same article, where sensors are inserted over each finger.

In this thesis, Ag NW networks are used as electromagnetic interference (EMI) shielding materials and transparent top and bottom electrodes for organic solar cells. Conductivity has great a contribution for EMI shielding as it absorbs the electric field component in the electromagnetic wave. Ag NWs are deposited onto different substrates in order to investigate their shielding properties. Through the use of different substrates, various EMI shielding application areas are elaborated. On the other hand, for solar cell electrodes, high transparency and conductivity are very important to improve charge collection and at the same time allow light to transmit to the device for maximum absorption. In order to demonstrate the feasibility of the replacement of

commercially available and industrial standard ITO films, Ag NW networks are used as both bottom and top electrodes in organic solar cells.

CHAPTER 2

ELECTROMAGNETIC INTERFERENCE SHIELDING OF SILVER NANOWIRE NETWORKS

2. 1. INTRODUCTION

Recently, large data transmission opportunity made communication devices that work within 1- 40 GHz electromagnetic (EM) wave range very attractive. Radar systems, mobile phones, transport systems and local area network (LAN) systems are prominent examples of this technology [7][8][9]. Development of EM technology increased the importance of electromagnetic interference shielding (EMI). Basically, EMI shielding means the reflection or absorption of EM radiation by a material that behaves as a shield against the penetration of high frequency radiation [10]. Through the use of a shield, data loss and data leakage can be prevented. Therefore, EMI shielding technology is very attractive for both commercial and military applications.

Pollution of EM radiation and EMI not only affects the electronic devices but also, have harmful effects on human health. Hence, researchers are continuously investing EM absorption properties of various materials in order to solve this problem [11][12][13]. EM wave absorbing materials can absorb those microwaves and convert them into thermal energy or dissipated microwave energy. In addition, these materials should be effective in a broad waveband, should show strong reflection and/or absorption behavior, should be light weight, thin and easy to use [14][15][16].

In this study, EMI shielding behavior of Ag NWs on different substrates are investigated. In order to enhance the shielding behavior, different substrates are selected and surface modifications are made through Ag NW decoration. Reflection and transmission properties of samples are investigated using a free space method within a frequency range of 18-40 GHz. Percent absorption and shielding effectiveness of the samples are calculated.

2. 2. THEORY AND LITERATURE REVIEW

2. 2. 1. Electromagnetic Waves

Discovery of EM waves was started upon the prediction of James Clerk Maxwell in 1864. By his mathematical approach, he founded the speed of light in vacuum and implied that light is an EM wave. As it is stated earlier by Faraday that changing magnetic flux induces electric field, EM wave is expressed as any disturbance in electric and magnetic field, which propagates with the speed of light in vacuum. Therefore, EM radiation is considered to be wavelike. It is produced by the acceleration of an electric charge and propagated by the periodic variation. It is the combination of electric field (E) and magnetic field (H) components, which are perpendicular to each other (Figure 2.1). EM wave travels with constant velocity (speed of light), which is related with the electric permittivity (ϵ_0) and magnetic permeability of a vacuum (μ_0) as shown in Equation 2.1.

$$c = \frac{1}{\sqrt{\epsilon_0 \mu_0}} \tag{2.1}$$

Frequency υ and the wavelength λ of the EM radiation are also a function of velocity as shown in Equation 2.2.

$$c = \upsilon\lambda \tag{2.2}$$

Frequency is expressed in terms of hertz (Hz) and 1 Hz equals to 1 cycle per second.
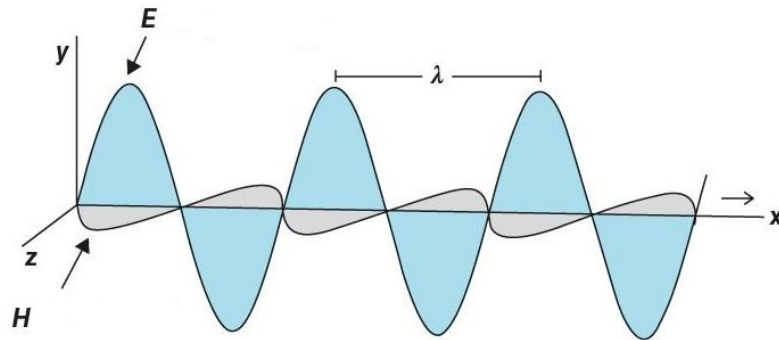
Figure 2. 1 Sinusoidal EM wave [17].

In the nineteenth century, Maxwell verified the wave nature of the EM radiation. Then in the beginning of the twentieth century, Planck and Einstein proved that EM radiation has particle like properties besides its wave properties. Therefore, EM radiation can be described as quantum energy packets, which are called photons. Photon energy can be calculated using the formula given below, where ν is the radiation frequency and h is the Planck's constant with a value of 6.62606×10^{-34} J (Equation 2.3) [17][18].

$$E = h\nu = \frac{hc}{\lambda} \qquad (2.3)$$

2. 2. 2. Electromagnetic Spectrum and Application Areas

EM spectrum shows the different type of EM waves in regions according to their frequency or wavelength (Figure 2. 2). Gamma rays, X-rays, ultraviolet, radio waves, infrared, microwaves are the form of the EM waves listed in the EM spectrum. From Equation 2.2, it is clear that frequency and wavelength of the EM wave are inversely proportional. Therefore, in EM spectrum as frequency increases, wavelength of the EM waves decrease. Moreover, from Equation 2.3, it can be stated that higher the frequency of the EM wave, higher the energy [18][19].
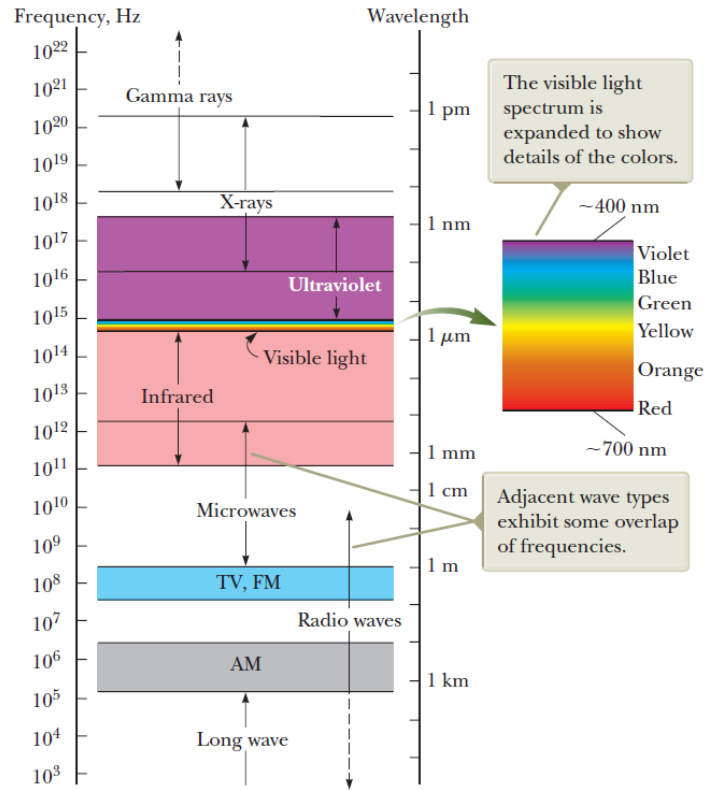
Figure 2. 2 Electromagnetic spectrum [18].

Radio waves: They are generated from the charges accelerated through conducting wires. They are generally used for broadcasting, communication and satellite transmissions. Their wavelengths range from 1 km to 0.1 m.

Microwaves: Like radio waves, they are also generated by electronic devices. They are used for cooking, communication and satellite transmission. Wavelength of microwaves ranges from 0.3 m to 10^{-4} m. Because of their short wavelengths, they are well suited for radar and satellite systems. Also, as they could be absorbed by water molecules, they could be used for cooking through heating these water molecules.

Infrared (IR): They are produced by molecules and objects at room temperature and absorbed by most materials. Absorbance of infrared energy, leads to an increase in the vibrational and translational motion of the materials atoms that heats the material. Wavelength of IR light ranges from 10^{-3} to 10^{-7} m. IR radiation is used in thermal imaging, remote controls, fiber-optics and short range communications.

Visible light (VIS): Only this part of the EM waves could be detected by human eye. Wavelength of visible light is between 400-700 nm and each wavelength corresponds to a different color. For instance, wavelength of blue is 400-430 nm, while the wavelength of red is between 625-700 nm. Visible light is used mostly for illumination and photography.

Ultraviolet (UV): The source of ultraviolet light is the sun. Wavelength of UV light ranges between 10^7-10^{-10}m. It is generally used at security marking, fluorescent lamps, detecting forged bank notes and sterilization.

X-Rays: They are produced by stopping the high energy electrons through bombardment over a metal target. Wavelengths of X-Rays range from 10^{-8} m to 10^{-12} m. They are used for treatment of cancer, as they could damage the living tissues. Moreover, X-rays are used for detecting the crystal structure of the unknown materials, as they have similar wavelengths compared with the atomic separation distance of solids. They are also used for the detection of bone breaks and security in order to observe the internal structure of objects.

Gamma Rays: It is emitted by radioactive nuclei during nuclear reactions. Wavelengths of gamma rays range from 10^{-10} m to 10^{-14} m. They are very dangerous and harmful for the living tissues. Therefore, it is used for detection and treatment of cancer [18][19].

2. 2. 2. 1. Microwave Band and Application Areas

Frequencies between 300 MHz and 300 GHz belong to microwaves. Their wavelengths range from 1 m to 1 mm. As seen in Figure 2.3, microwaves can be divided into several bands according to their frequency and application areas. According to Table 2. 1, radar and satellite are the main application areas for microwaves [20]. In this thesis, measurements are carried out between a frequency range of 18 and 40 GHz.
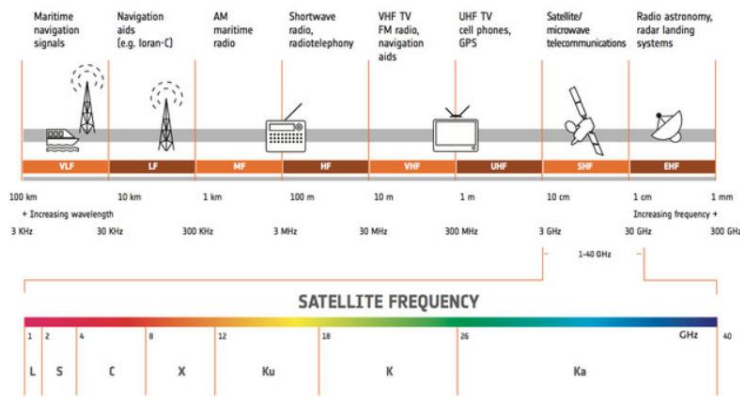
Figure 2. 3 Bands between 3 KHz and 300 GHz [20].

Table 2. 1 Radar and satellite bands and their application areas [20].

Name of the Band	Frequency Range	Application Areas
L - Band	1 - 2 GHz	Global Positioning System (GPS), Satellite Mobile Phones
S - Band	2 - 4 GHz	Weather radar, Surface ship radar Communication satellite (NASA)
C - Band	4 - 8 GHz	Satellite communication Full-time satellite TV networks
X - Band	8 - 12 GHz	Primarily used by military Civil, military, government inst. for weather monitoring Air traffic control, Defense tracking Vehicle speed detection
Ku - Band	12 - 18 GHz	Satellite communication
K - Band	18 - 27 GHz	Water vapor absorption
Ka - Band	27 - 40 GHz	Communication satellite, High resolution mapping, Airport surveillance, Close range targeting on military aircraft

2. 2. 3. Electromagnetic Wave - Material Interaction

When EM wave faces a material, there are three possible ways of interaction. It can be transmitted through the material (T), absorbed by the material (A) or get reflected from the material (R). As, EM waves produced from electronic sources contain both electric and magnetic field, electrical and magnetic properties of the material are responsible in determining these three occurrences. According to energy conservation principle, sum of the fractions of reflected power (P_R), transmitted power (P_T) and absorbed power (P_A) with respect to the power of the incident wave should be equal to one, as shown below in Equations 2.4 and 2.5.

$$1 = R + T + A \qquad (2.4)$$

$$1 = \frac{P_R}{P_0} + \frac{P_T}{P_0} + \frac{P_A}{P_0} \qquad (2.5)$$

For reflection to occur, material should have mobile charge carriers (electrons and holes) that provide conductivity [10]. For absorption, incident EM power should be damped by the material and material should contain both magnetic and electric dipoles. These power losses due to EM wave-material interaction can be categorized into three main groups. Energy absorption can be realized through polarization of dipoles (dielectric loss), movement of magnetic domains (magnetic loss), flow of free electrons (conductance loss).

Dielectric materials have bound negative and positive charges, which are not free to move. Therefore, they are insulators. When dielectric materials are subjected to EM wave, the external electric field allow them to store the electrical energy by the shift of negative and positive charges (Figure 2. 4.).
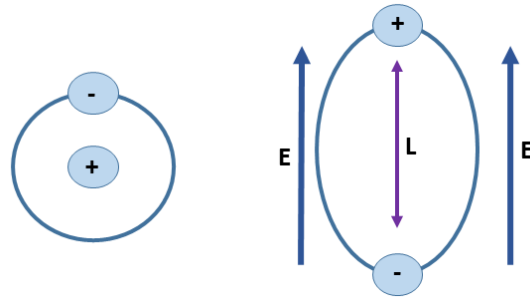
Figure 2. 4 Typical atom in the absence of (left) and under an applied electric field (right) [21].

When, conductive materials are subjected to an electric field, electric dipoles within the material interacts with the incident wave. Similarly, when EM wave interacts with conductive materials, electric field component of the EM wave couples with the free electrons and the EM energy is absorbed.

Similar to behavior of conductive materials in applied electric field, when magnetic materials are subjected to magnetic field, magnetic dipoles are aligned within the material. Diamagnetic and paramagnetic materials are considered as non-permanent magnetic materials. They show small magnetization only when an external field is present. When external field is applied to diamagnetic materials, their electron orbital motion changes. Occurred internal magnetic field is opposite to the applied external magnetic field. For the case for paramagnetic materials, they contain permanent atomic dipoles. With the applied field, these dipoles get aligned. On the other hand, ferromagnetic materials (i.e. iron, nickel and cobalt) have permanent magnetic moments even in the absence of an external field. [21].

2. 2. 3. 1. Electromagnetic Wave-Nanomaterial Interaction

Nanomaterials show unique electrical, magnetic and optical properties. When compared to their bulk forms, nanomaterials have much more active atoms on their surface. Therefore, dielectric loss caused by interface polarization is larger. For the case of magnetic loss, if the size of the conductive nanoparticle is too small, due to change in the magnetic flux, eddy current generation would be higher. This results in higher absorption values [22]. Generally, maximum penetration depth of EM waves

12

are 1 µm in conductive materials at 10 GHz [22]. Therefore, nanomaterials show great absorption properties.

2. 2. 4. Electromagnetic Shielding Theory

Within the recent years, the number of electronic devices that we use daily is increased significantly. All those devices generate and release EM waves. When these released EM energies are transmitted from one electronic device to another via radiated or conducted paths, it is called as electromagnetic interference (EMI). As every system has its own EM interference inside, they have their own electromagnetic compatibility (EMC). It is set in order to operate electronic devices safely in their intended EM environment without suffering from or causing unacceptable degradation. By shielding and filtering, EM energy could be reduced [23].

Therefore, it is clear that the demand for EM shielding is highly increasing in the developing world. Shielding occurs mainly by two mechanisms, that are reflection and absorption. According to the substrate of the shielding material, reflections at various surfaces or interfaces in the shield should be considered as multiple reflections.

According to Scnelkunoff's formulation, plane wave shielding effectiveness can be expressed as the sum of absorption loss (A), reflection loss (R) and multiple reflections (M), as shown in Figure 2.5 [24].
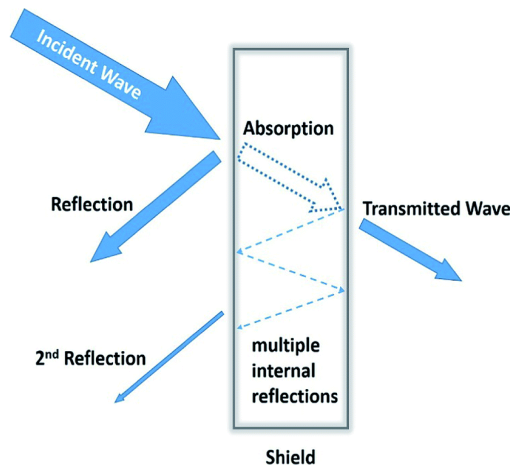
Figure 2. 5 EM wave- material interaction [24].

Both components of EM wave, electric and magnetic field components interact with the shield. Some part of the field is reflected, some part of the field is absorbed and the remainder is transmitted. Reflection occurs due to materials with different electric and magnetic properties and the absorption occurs due to energy losses within the shield. Both electric and magnetic losses are clarified in the previous part of this thesis named "Electromagnetic Wave - Material Interaction". For an effective shield material, transmission is expected to be minimum. If the shield is to be used at low frequencies, reflection and absorption should take place as shielding mechanisms. However, for high frequency applications, absorption dominant shielding mechanisms are desired. Shielding effectiveness of the material can be calculated by the obtained reflection and transmission loss. The reflection (R) and the transmission (T) ratios are obtained from the network analyzer measurements in the form of scattering parameters "S_{mn}". The first letter "m" indicates the network analyzer port receiving the EM power and the second letter "n" indicates the port that is transmitting the incident energy. Vector network analyzer gives the 4 scattering parameters as S_{11}, S_{12}, S_{21}, S_{22} and values are given as magnitude (dB) and phase (θ) (Figure 2. 6) [25] .
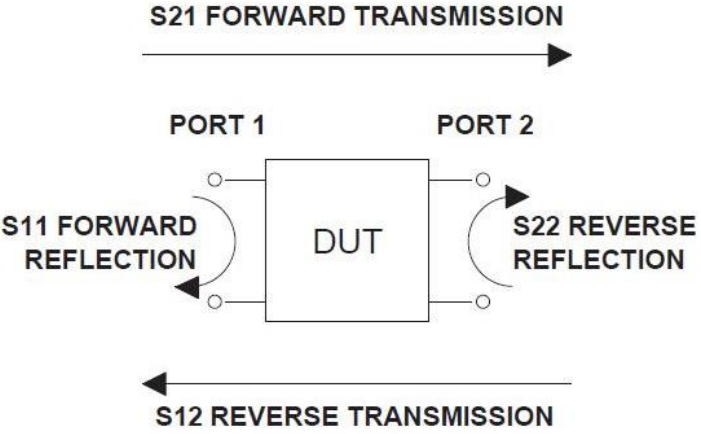
Figure 2. 6 Scattering parameters [25].

For instance, in one of the EM measurement methods called free space method, two horn antennas, a network analyzer and a lens system are used. Power waves are emitted and received by the antennas and the scattering parameters are obtained. Reflection loss is obtained as S_{11} (dB), which is the data of the electromagnetic waves emitted from horn1 and reflected back to horn1. If the measurement was made from horn2, it

is called as S_{22}. On the other hand, transmission loss was obtained as S_{21} (dB) when the EM wave is emitted from horn1 and transmitted to horn2. If the transmitted EM wave measurement is made from horn1, it is called as S_{12}. These S parameters are logarithmic functions as shown in Equation 2.6 and 2.7 below.

$$\text{Reflection loss (dB)} = S_{11} = 10 \log(\frac{P_R}{P_i}) \qquad (2.6)$$

$$\text{Transmission loss (dB)} = S_{21} = 10 \log(\frac{P_T}{P_i}) \qquad (2.7)$$

From network analyzer data, the ratio of the transmitted power (P_T) to incident power (P_i) and ratio of reflected power (P_R) to incident power (P_i) can be calculated using Equation 2.8 and 2.9. From this ratio, percent absorption can be easily derived using Equation 2.10 [26].

$$\text{Reflection \%} = \frac{P_R}{P_i} \text{x} 100 = 10^{\frac{S_{11}}{10}} \text{x} 100 \qquad (2.8)$$

$$\text{Transmission \%} = \frac{P_t}{P_i} \text{x} 100 = 10^{\frac{S_{21}}{10}} \text{x} 100 \qquad (2.9)$$

$$\text{Absorption \%} = \left(1 - 10^{\frac{S_{11}}{10}} - 10^{\frac{S_{21}}{10}}\right) \text{x} 100 \qquad (2.10)$$

Moreover, through the use of effective absorbance term (A_{eff}), amount of absorbed EM wave within the shield can be calculated using Equation 2.11 [26].

$$A_{eff} = \frac{1-R-T}{1-R} \qquad (2.11)$$

Shielding effectiveness is the summation of all contributions from reflection (SE_R), absorption (SE_A) and multiple reflection (SE_M), as shown in Equations 2.12 and 2.13.

$$\text{SE total (dB)} = 10 \log(\frac{P_t}{P_i}) = 20 \log(\frac{E_t}{E_i}) = 20 \log(\frac{H_t}{H_i}) \qquad (2.12)$$

$$\text{SE total (dB)} = SE_R + SE_A + SE_M \qquad (2.13)$$

All three mechanisms can be calculated individually using Equations 2.14, 2.15 and 2.16.

$$SE_R = 10 \log(1 - R) \qquad (2.14)$$

$$SE_A = 10 \log(\frac{T}{1-R}) \qquad (2.15)$$

$$SE_M = 20 \log(1 - 10^{\frac{SE_A}{10}}) \qquad (2.16)$$

Besides all, EMI shielding efficiency term presents the materials ability to block waves in terms of a percentage. EMI shielding effectiveness (dB) is converted into EMI shielding efficiency (%) using Equation 2.17 [26].

$$\text{Shielding efficiency \%} = 100 - \left(\frac{1}{10^{\frac{SE}{10}}}\right) \text{x } 100 \qquad (2.17)$$

Table 2.2. shows several shielding effectiveness (dB) values and corresponding shielding efficiencies in percentage.

Table 2.2 Shielding efficiency conversion [24].

Shielding Effectiveness (dB)	Shielding Efficiency (%)
0	0
10	90
20	99
30	99.9
40	99.99
50	99.999
60	99.9999
70	99.99999
80	99.999999
90	99.9999999

To conclude, electromagnetic interference shielding effectiveness (EMI SE) is a measure of material's ability to block EM waves. In order to determine the EMI SE, there are several factors that should be considered such as [23]:

- Frequency of the EM field,
- Shield material properties (conductivity, permeability, permittivity),
- Shield thickness and
- Type of the EM field source (plane wave, electric field, magnetic field).

2. 2. 5. Electromagnetic Interference Shielding Materials

Today's shielding technology is derived from the early introduced concept of Faraday back in 1821. It is known as Faraday's cage, which is a conductive enclosure having zero electrical field inside. When an external electric field is applied, it causes the electric charges within the conductive material to be distributed. Therefore, the field inside the cage is cancelled. Through the use of this effect, sensitive electronic equipment is protected from external radio frequency interference (RFI). Faraday cages are also used to protect radio transmitters against RFI and protect people and equipment against lightning strikes and electrostatic discharges. However, Faraday cages cannot block slowly varying magnetic fields.

For materials to be used as EMI shields, they should prevent the penetration of EM wave. In order to act as a shield, they should reflect or absorb the EM wave as shown in Figure 2.7.

Material	Penetration
TRANSPARENT Low loss insulator	Total
OPAQUE Conductor	None All reflected
ABSORBER Lossy insulator	Partial Total
ABSORBER Mixed Matrix= low loss insulator Particles=absorbing materials	Partial Total
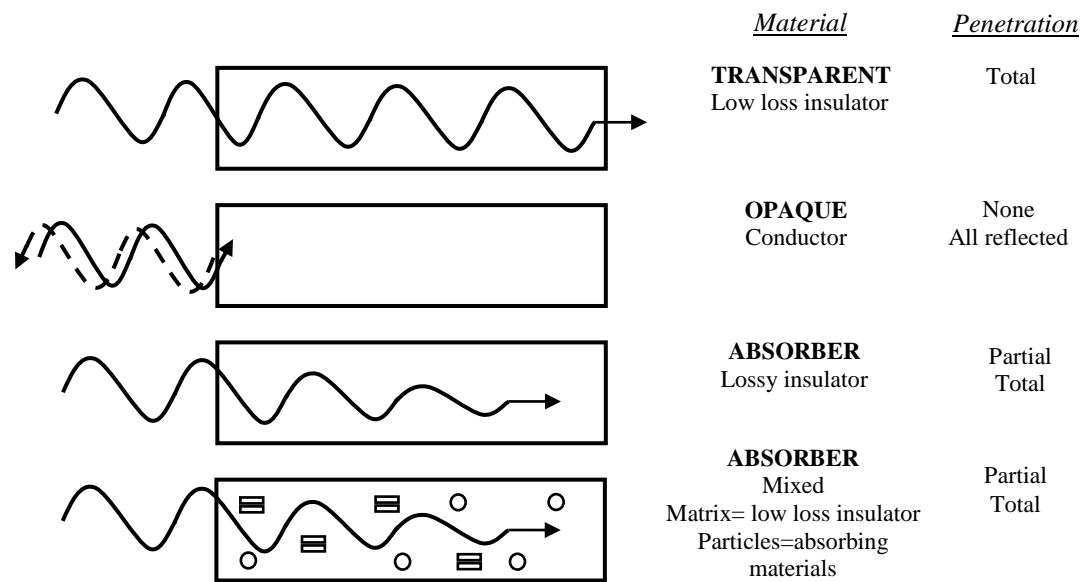
Figure 2. 7 Schematics of EM wave-material interactions.

Firstly, selected materials should be conductive to show reflectance loss. Therefore, generally metals are selected as they have free electrons for conductivity. To illustrate, metals like silver (Ag), copper (Cu), gold (Au), aluminum (Al) are great candidates for reflection due to their high conductivity. They are used in the form of bulky metal sheets, metal screens and metal foams. For RF shielding, metallic inks of nickel (Ni) and copper (Cu) are preferred. If the substrate is an insulator, then metal coatings are preferred. For the deposition of metallic coatings, generally electroplating, electroless plating and vacuum deposition methods are used. Although conductivity is obtained, poor scratch and wear resistance do remain as major problems for metallic coatings.

Secondly, maintaining electric and magnetic dipoles will increase the EM wave-material interactions. Proportional to these interactions, absorption loss increases. Barium titanate ($BaTiO_3$) or other materials with high dielectric constants can be used for electric dipoles, while magnetite (Fe_3O_4) and other materials with high magnetic permeability can be used for magnetic dipoles. Therefore, absorption loss is proportional to electrical conductivity and magnetic permeability of the shield material. Absorption loss increases with the thickness of the shield. This is because the

time that EM wave travels through the shield increases. However, at high frequencies EM wave penetrates only the near surface region of the electrical conductor. This leads to the skin effect. When EM wave interacts with the surface of conductor. It penetrates only the near surface and drops exponentially with increasing distance towards the depth of the conductor. It can be stated that skin depth (Equation 2.18) decreases by
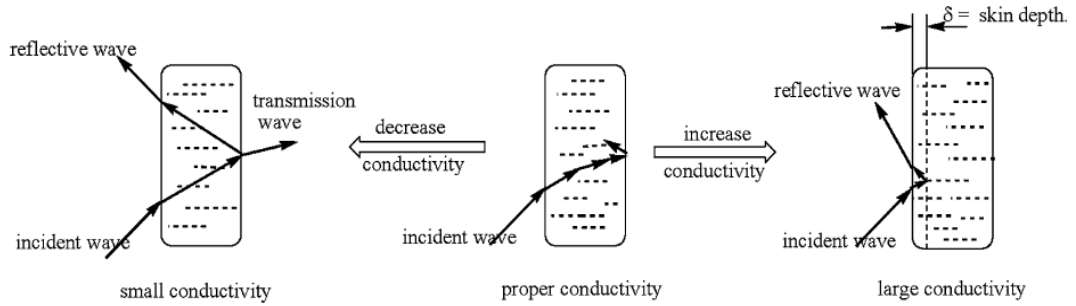
Figure 2. 8 EM wave transmission model for materials with different conductivities [22].

increasing frequency, conductivity and permeability as shown in Figure 2.8 [10].

$$\text{Skin depth } \delta = \frac{1}{\sqrt{\pi f \mu \sigma}} \qquad (2.18)$$

,where f is frequency (MHz), μ is magnetic permeability ($= \mu_0 \mu_R$), μ_R is relative magnetic permeability, $\mu_0 = 4\pi \, x 10^{-7}$ H/m and σ is electrical conductivity in Ω/m.

Thirdly, in order to increase the EM wave - material interactions, multiple reflections can also be utilized. For this method, shield material should have various surfaces or interfaces in order to increase the amount of inner reflections. EM wave scatters from those surfaces and the intensity of the wave decreases. For this purpose, foam materials with large pores are used as substrates. In addition, composite materials with large interfaces can also be used [10]. However, SE value obtained from multiple reflections can be eliminated if the absorption is larger than 10 dB, multiple reflection term can be neglected.

Materials containing Ag NWs) and silver nanoparticles (Ag NPs) as conductive fillers are used as EMI shielding materials in literature. Zhao et. al. used Ag NPs in order to reduce the contact resistance between multi-walled carbon nanotubes (MWNTs) [27]. They used in-situ photochemical reduction method for decorating Ag NPs over

MWNT sheets. With an increase in conductivity from 27.7 to 40.0 S∕cm, EM SE is increased from 18.7 to 45.5 dB within frequency range of 15-40 GHz. SE of one layer MWNT sheet approached the value of 20.3 dB, which is the limit for commercially used EMI shielding materials [21]. Moreover, single layer MWNT sheet with a thickness of 68 μm showed greater effectiveness compared to Ni mesh. Main reason for this high SE is the small diameter and larger aspect ratio of MWNTs. Moreover, high conductivity of the Ag NP decorated MWNTs weakened the incident EM wave through the depth of the conductor [23]. On the other hand, Yu et. al. compared EMI shielding properties of Ag NW and Ag NP conductive composites [28]. Firstly, films with high electrical conductivity were prepared both with Ag NWs and Ag NPs. Ag NW/epoxy composite had a SE of 25.09 while Ag NP/epoxy having the same parts per hundreds part of resin value (phr) had a SE of -5.06. It was concluded that the Ag NW /polymer composites exhibit better SE compared to those with Ag NPs due to the high aspect ratio of Ag NWs. In literature, shielding behavior of Ag NWs were investigated in low frequency ranges. Ma et. al. investigated EM shielding behavior of the ultra-light weight composites containing Ag NWs and polyimide within a frequency range of 30 MHz- 1.5 GHz [29]. Three dimensional network of Ag NWs is maintained over the foam fabricated through one pot liquid foaming process. Ag NW decorated foam having 7.8 wt. % Ag NW showed an EMI SE of 30 − 9 dB over a frequency range of 30 MHz − 1.5 GHz. Main reason for this behavior was the reflections of interconnected Ag NW networks on the surface and inside the foam combined with the multiple reflections. Fang et. al. investigated the shielding behavior of Ag NW/polyaniline (PANI) composite films within a frequency range of 8 - 12 GHz [30]. Free standing composite films were prepared by a novel method. As a first step, Ag NW/n-butanol dispersion was cast on the glass slide. Then as a second step, the PANI/ N-Methyl-2-pyrrolidone solution was cast on the top of the Ag NW layer. Layers were cured under infrared light and released from the glass substrate by soaking in water. Moreover, a Ag NW/PANI composite film was prepared using direct mixing method for comparison. As prepared structure having 14 vol. % Ag NWs showed an excellent EMI shielding efficiency of above 50 dB over a wide band range of 1.2 GHz, while the one made by direct mixing method showed an EMI shielding efficiency of above 50 dB only over a narrow bandwidth of 0.4 GHz.

In this thesis, EM shielding behavior of Ag NWs are investigated within a frequency range of 18-40 GHz. As a substrate, polyethylene terephthalate (PET), cotton textile, filter paper and felt were selected. In order to obtain a two dimensional network of Ag NWs, spray coating method was used. On the other hand, to obtain a three dimensional network of Ag NWs dip coating method was utilized.

2. 2. 6. Characterization with Free Space Method

For the characterization of EM wave - material interaction and EM properties of materials the two most commonly used methods are waveguide and free space method. For the waveguide method, a hollow metallic circular tube is used. EM wave is sent from one point. The wave is propagated by reflecting from the inner walls of the tube. So, the EM energy is transferred from one part to another. There are different versions of the waveguide method. Although they are generally the same, either the inner reflection mechanisms or the specimen shapes are different. For the free space method, two horn antennas, a network analyzer and a lens system are used as shown in Figure 2.9. Power waves are emitted and received by the antennas and the scattering parameters are obtained. Condensing lenses focus emitted waves on the sample surface, which is placed between the lenses [24]. Compared to waveguide method, sample sizes are relatively larger in order to avoid diffraction effects [31]. During the measurements, network analyzers are used. They are generally used to measure the network parameters of electrical networks. For this work, scattering parameters for reflection and transmission are characterized within desired frequency range. There are two types of network analyzers that are commonly in use. Scalar network analyzers (SNA) measures the amplitude properties only, whereas vector network analyzers (VNA) measures both the amplitude and phase properties [32]. VNA is selected for characterization in this thesis.
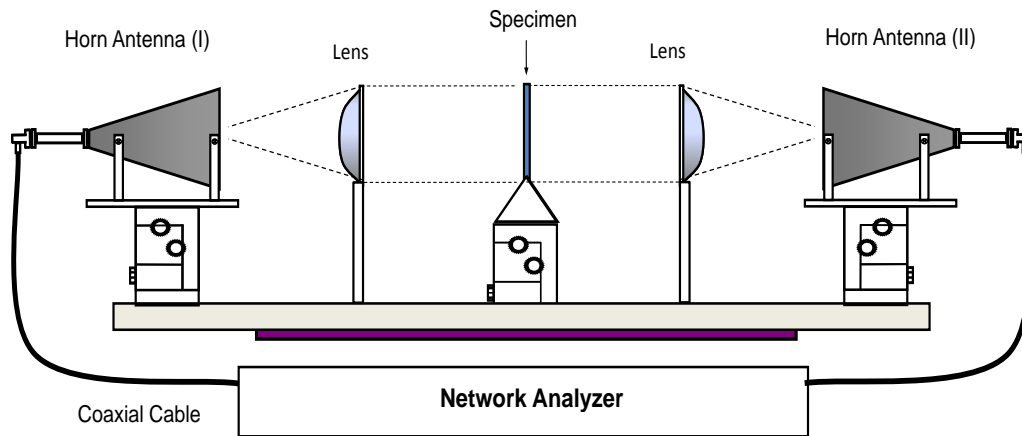
Figure 2. 9 A schematic of the free-space measurement set up [31].

For the measurement of SE, signal levels are compared with and without the sample. In order to obtain better results, reference measurements and the measurements with the metal reflector must be made. During reference measurements, air is measured and during measurements with a reflector, reflected signal is measured. By these measurements, electrical and magnetic properties of the materials can be easily determined [29].

In this thesis, free-space method is used for the characterization. It is a non-destructive and contactless method and it is more convenient to measure complex and inhomogeneous samples. Calibration should be made prior to each measurement to obtain accurate results [30].

2. 2. 6. 1. Short-Open-Load-Thru (SOLT) Calibration

It is the simplest method for the calibration. It requires short circuit, open circuit, 50 ohm load and through connection. These loads are present in the calibration kit of the VNA. This calibration is used to eliminate the systematic errors. Therefore, calibration of cables and connectors are made at each step. The aim is to make measurements with respect to required reference planes. [33].

2. 2. 6. 2. Through- Reflect- Line (TRL) Calibration

It is preferred for the non-coaxial devices at microwave frequency band. Through standard is applied by maintaining an equal distance between both antennas and the sample holder. Reflect ion standard is obtained by placing a metal plate between the antennas. While placing the plate, thickness of the plate is considered and one of the antennas is pulled backwards by a distance equal to the thickness of the plate in order to maintain equal distance between antennas and the sample. Line standard is achieved by placing one of the antennas at the quarter of the wavelength of the free-space. By this calibration, reflections from outside are minimized [33].

2. 3. EXPERIMENTAL DETAILS

2. 3. 1. Polyol Synthesis of Silver Nanowires

All chemicals used in the synthesis of Ag NWs were supplied from Sigma-Aldrich and used without any purification. Ag NWs were synthesized according to the procedure reported by Coskun et al [34]. Synthesis had two steps. At the first step, poly (vinylpyrrolidone) (PVP, molecular weight = 55000), ethylene glycol (EG) and sodium chloride (NaCl, 99.5 %) were used. First, a 10 ml of solution containing 0.45M EG/PVP was prepared. Then 7 mg of NaCl was added into this solution. The solution was heated up to 170 °C in an oil bath and stirred with a magnetic stirrer at 1000 rpm to obtain homogeneous solution. In the meantime, second step of the synthesis was carried out, which was the preparation of the Ag source. For this step, ethylene glycol (EG) and silver nitrate ($AgNO_3$) were used. A 5 ml of solution containing 0.12 M $AgNO_3$ (99.5%) in 5 ml EG was prepared. Then, this solution was added drop-wise into the PVP solution by an injection pump (Top-5300 Model Syringe Pump) at a rate of 5 ml / hr. During the addition of Ag^+ ions into the solution, Ag NPs start to form via homogeneous nucleation. PVP molecules passivate the (100) plane of the nanowires and leaves (111) as an active plane for a directional growth. Therefore, anisotropic growth along [110] direction was obtained. Once the addition process is completed, solution was annealed for 30 minutes at 170 °C and finally air cooled to room temperature. Solution was purified afterwards. For this, the solution was firstly diluted

with acetone in order to separate remaining PVP and EG from the Ag NWs and centrifuged at 7000 rpm for 10 minutes. Remaining Ag NWs were dispersed in ethanol and centrifuged at 7000 rpm for 10 minutes for further purification. Lastly, the solution was dispersed in ethanol and with the several decantation steps, purified Ag NWs were obtained [34].

2. 3. 2. Fabrication of Silver Nanowire Networks on PET Substrate

For first experiments, PET foils was used as the substrate. It is the fourth most produced polymer and is environmentally friendly as it can be recycled. It has high optical transmission, great flexibility and is compatible with the solvents used in this work. PET foils having 250 μm thickness were used. They were cut into 8 cm x 8 cm squares. All substrates were cleaned and sonicated with acetone (99.8%), isopropyl alcohol (99.8%) and finally deionized water (18.3 MΩ) for 15 minutes each. Then, substrates were placed over a hot plate heated to 150°C for the instant removal of ethanol. Then ethanolic Ag NW solution was deposited over the PET substrates using a simple nitrogen (N_2) fed air brush. All spray coating processes were carried out at a N_2 pressure of 2 atm and at a spraying distance of 10 cm from the hot plate.

Spray coated nanowire density determines both the optical transmittance and the sheet resistance of the network. PET substrates were coated with different densities of Ag NWs having sheet resistances of 10 ohm/square, 100 ohm/square, 1 kohm/square, 10 kohm/square and 100 kohm/square.

2. 3. 2. 1. Metal Evaporation over Ag NW Networks on PET Substrate

In order to decrease the transmittance of the incident wave, thin metallic films were deposited onto Ag NW/PET substrates using physical vapor deposition (PVD) technique. For this purpose, 5, 10 and 20 nm of Ni thin films were deposited over Ag NW networks on PET substrates using Nanovak NVTH-350 thermal evaporator at a base pressure of 1.5×10^{-6} Torr.

2. 3. 3. Fabrication of Ag NWs on Textile

As an alternative substrate, at this part of the thesis, 100 % cotton fabrics were used. After sonication with ethanol, substrates were dip coated in ethanolic Ag NW solution and dried. Number of dip coating cycles determine the resistance of the substrates due to an increase in the nanowire density over the substrate. This procedure was repeated until the desired resistance is obtained. Four specimens with different resistance values of 1 mohm, 10 kohm, 1 kohm and 100 ohm were prepared.

2. 3. 4. Fabrication of Ag NWs on Filter Paper

Whatman 1001-185 filter papers with a pore size of 11 µm were used for this process. Substrates were cut in square shapes with dimensions of 8 cm x 8 cm. Substrates were sonicated with ethanol (99.8 %) as a cleaning step before dip coating. Then they were dip coated with ethanolic Ag NW solution for 10 minutes and dried at 80 °C for 5 minutes. Four specimens with different resistance values 10 kohm, 1 kohm, 100 ohm and 10 ohm were prepared.

2. 3. 5. Fabrication of Ag NWs on Felt

Felt is a kind of textile made by rolling and pressing wool or fibers. Moisture and heat are applied during the process to create a smooth surface. For the deposition of Ag NWs, the same procedure used for the decoration of textile and filter paper was utilized. Following sonication with ethanol, substrates were dip coated using ethanolic Ag NW solution and dried. Upon deposition of Ag NWs, felts with resistances of 1 mohm, 10 kohm, 1 kohm and 100 ohm were obtained.

2. 4. CHARACTERIZATION METHODS

2. 4. 1. Scanning Electron Microscopy (SEM)

Synthesized Ag NWs were analyzed using field emission scanning electron microscopy (FE-SEM) (Nova NanoSEM 430). SEM samples were prepared by drop casting of ethanolic Ag NW solution over pre-heated Si wafers. Else, Ag NW networks on substrates were used directly for SEM characterization.

2. 4. 2. Transmittance Measurements (UV-VIS)

Agilent 8453 UV-VIS spectrophotometer was used to measure the direct transmittance of the Ag NW/PET samples and Ni/PET samples within the wavelength range of 400 and 700 nm.

2. 4. 3. XRD Analysis

Rigaku D/Max-2000 PC diffractomer was used for X-Ray diffraction (XRD) analysis of Ag NWs. Diffractomer was used with Cu Kα radiation (λ=1.54 Å) at operating voltage of 40 KV. A 2θ range of 30-60° at a scanning rate of 2°/min was employed.

2. 4. 4. Characterization of EM Wave Sample Interaction by Free-Space Method

Free-Space method was used for the EM characterization of the Ag NW/PET, Ni/Ag NW/PET, Ni/PET, Ag NW/filter paper, Ag NW/textile and Ag NW/felt samples. This method was used for the measurements since it is easy and gives accurate results on inhomogeneous and anisotropic media. Reflection and transmission values were obtained as both magnitude (dB) and phase angles (degree) using Vector Network Analyzer. Measurements were made within a frequency range of 18-40 GHz (K and Ka - Band). Scattering parameters (S11, S21, S22, S21 and phases) were obtained.

From those values, percent absorption was calculated using Equation 2.18 based on the principle of conservation of energy. SE values were also deduced for each sample using Equations 2.22, 2.23 and 2.24. Before each measurement, TRL calibration was made. Moreover, for each sample four measurements were carried out and the average of these measurement results was used for the calculations. During each sample set, reflection and transmission loss of air and the reflector were measured in order to observe whether if there was a change or not. It was important since measurements were made using free-space (Figure 2.10), meaning that it was open to any changes.

Figure 2. 10 Photograph of free space measurement setup used in this thesis.

2. 5. RESULTS

2. 5. 1. Characterization of Silver Nanowires

Ag NWs were synthesized using polyol method. After the purification step, nanowires were characterized using SEM. A representative SEM image of Ag NWs is provided in Figure 2.11.
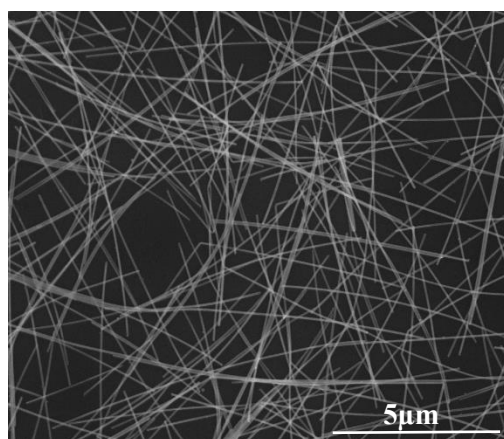
Figure 2. 11 A SEM image of synthesized Ag NWs.

Length and diameter analysis of NWs were made by measuring 100 nanowires from the SEM images. According to this analysis, average diameters and length of NWs were determined as 50 nm and 8 µm, respectively.
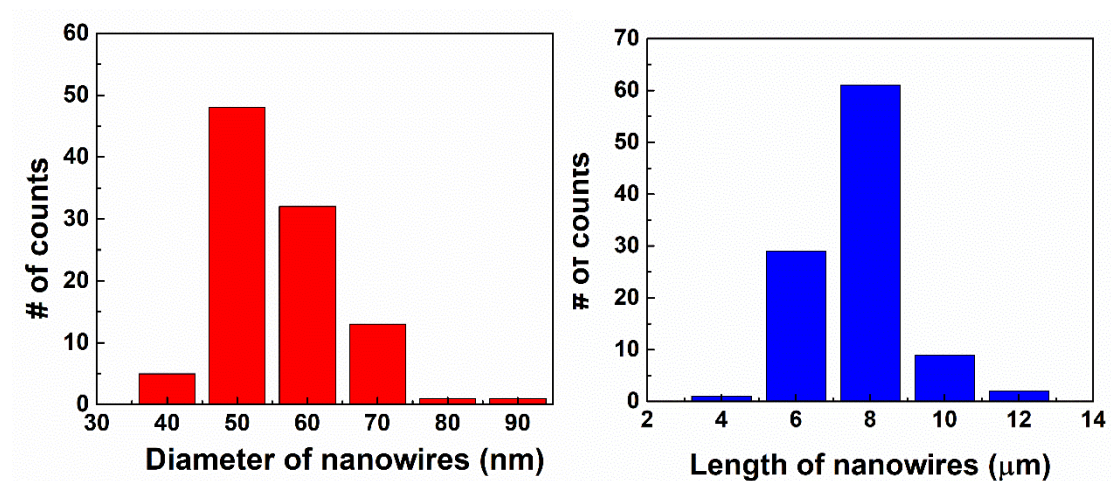
Figure 2. 12 (a) Diameter and (b) length distribution of the synthesized Ag NWs.

In order to determine the purity of as synthesized Ag NWs, XRD analysis was carried out. A typical XRD pattern is provided in Figure 2.13 and no impurities were detected within the NWs under the detection limit of XRD apparatus (JCPDS Card No. 04-0783).
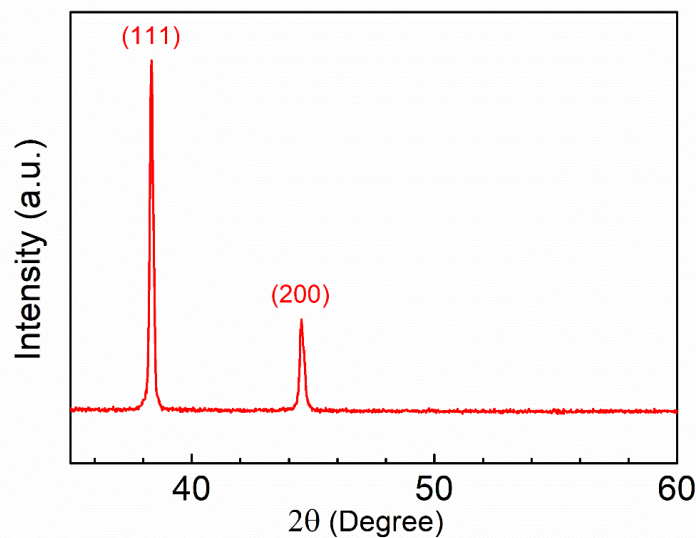
Figure 2. 13 XRD pattern for synthesized Ag NWs.

2. 5. 2. Silver Nanowire Networks on PET

Purified Ag NW solution was used for spray coating over PET substrates. 5 different samples with different conductivities were prepared. A home-made bending/stretching setup was used to determine flexural durability of Ag NW networks on PET substrates. Samples were bent both in tension and compression mode for 1500 cycles each and the change in the resistance of networks normalized to initial resistance is measured and provided in Figure 2.14. It was evident from these results that the adherence of Ag NWs to each other and to the PET substrates were remarkable.
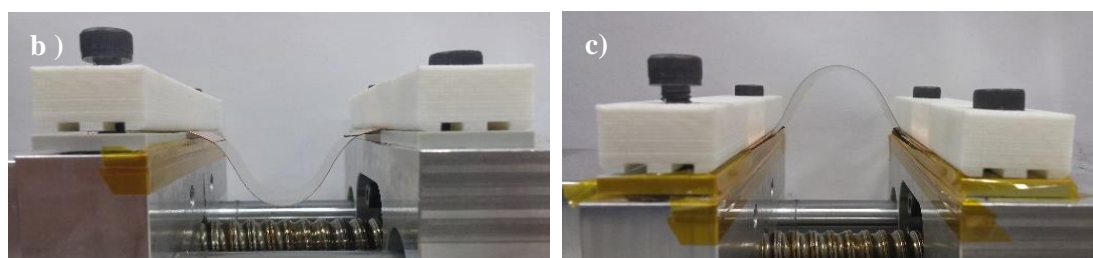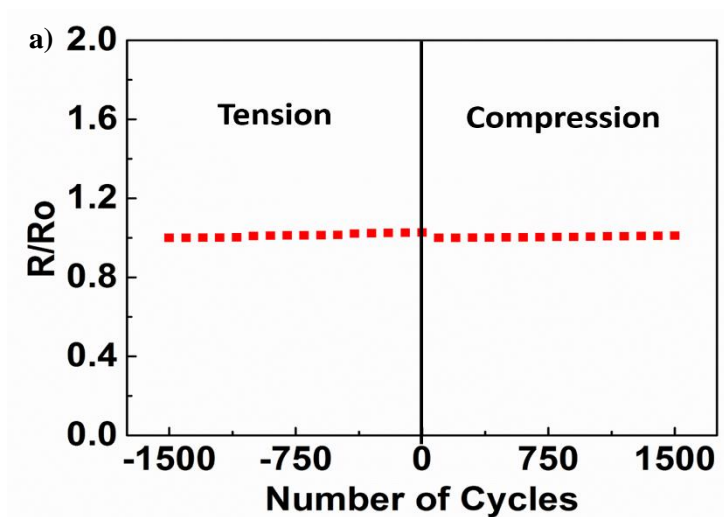
Figure 2. 14 (a) Resistance change with the number of bending cycles and photograph of the samples under (b) tension and (c) compression.

Optical transparency was the other important parameter for networks. A UV-VIS setup was used for the analysis of transparency of networks. First, optical transmittance of the bare PET substrate was measured. Then Ag NW deposited samples were measured by subtracting the value of the bare PET substrate to obtain optical transmittance of the Ag NW coating. Wavelength dependent optical transmittance of the fabricated samples is provided in Figure 2.15. Optical transmittance of the samples was found to decrease with increased resistance. Increased Ag NW density over PET substrates blocked the light, decreased transmittance of the networks. It was also clear from Figure 2.15 that desired conductivity and optical transmittance can be simply adjusted by the number spraying coating.
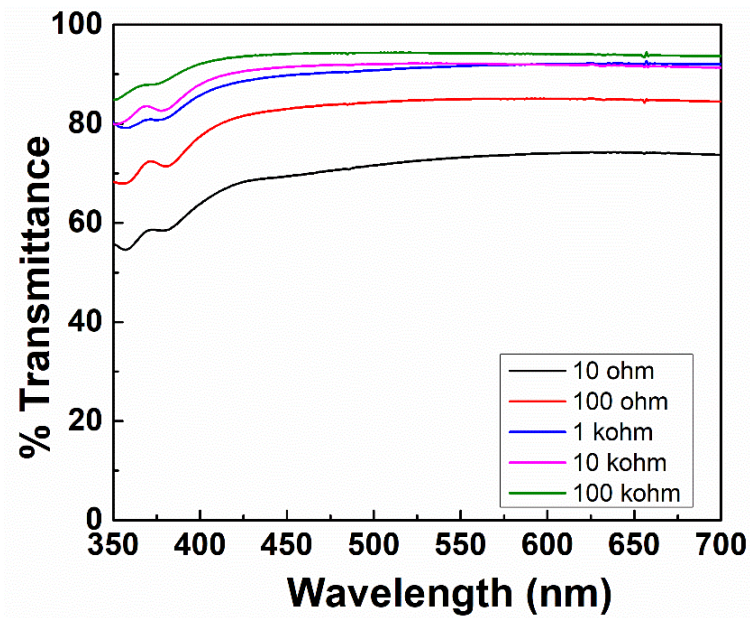
Figure 2. 15 Optical transmittance of fabricated Ag NW networks with different sheet resistances.

Samples with the highest and the lowest sheet resistance values were examined by SEM, images of which are provided in Figure 2.16 (a) and (b) respectively. When these images are compared, it is clear that the nanowire junction points increase with nanowire density. As the number of charge transport paths increase, the resistance of the network decreases.
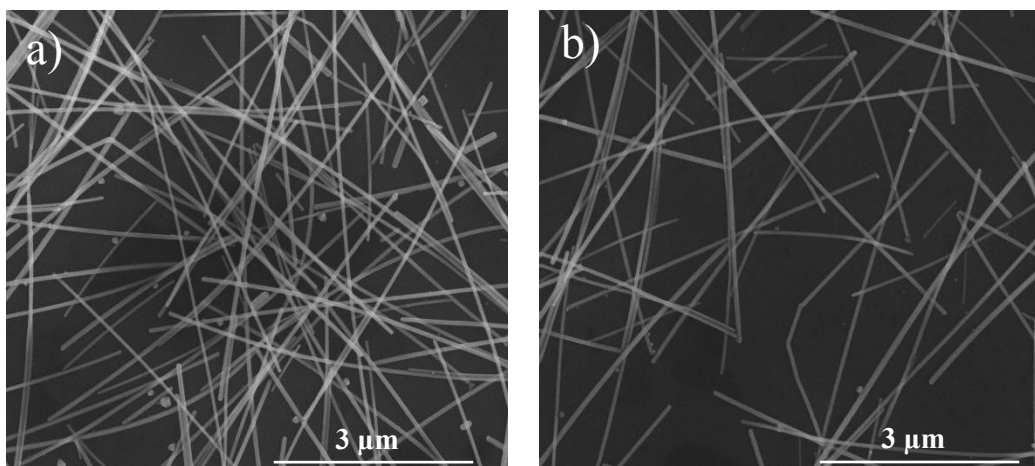
Figure 2. 16 SEM images of Ag NW networks with resistances of (a) 10 ohm and (b) 100 kohm

EM measurements of samples were made and S parameters were obtained. S parameters were briefly introduced at previous sections and in Figure 2.6. S_{11} values showed the reflection (Figure 2. 17) and S_{21} values showed the transmission of samples (Figure 2. 19). It can be stated from Figure 2. 17 that empty PET do not reflect the EM wave. The conductivity of the network was increased with the density of Ag NWs deposited onto PET. It can be stated that the reflectance of the EM wave was increased proportionally with conductivity. Samples with sheet resistances of 10 ohm and 100 ohm showed similar behavior to a metal reflector. Almost all of the incident wave was reflected from those samples. Moreover, in order to control the EM shielding behavior of the fabricated samples, sample with 100 ohm sheet resistance was rotated clockwise for 90 degrees. No change was observed within the reflectance spectra of the sample, as shown in Figure 2. 18. Maximum difference obtained from this rotation operation was measured as 0.4 dB. Transmittance spectra of the fabricated samples is provided in Figure 2.19. Low transmittance and a reflection dominant shielding was observed for these samples.
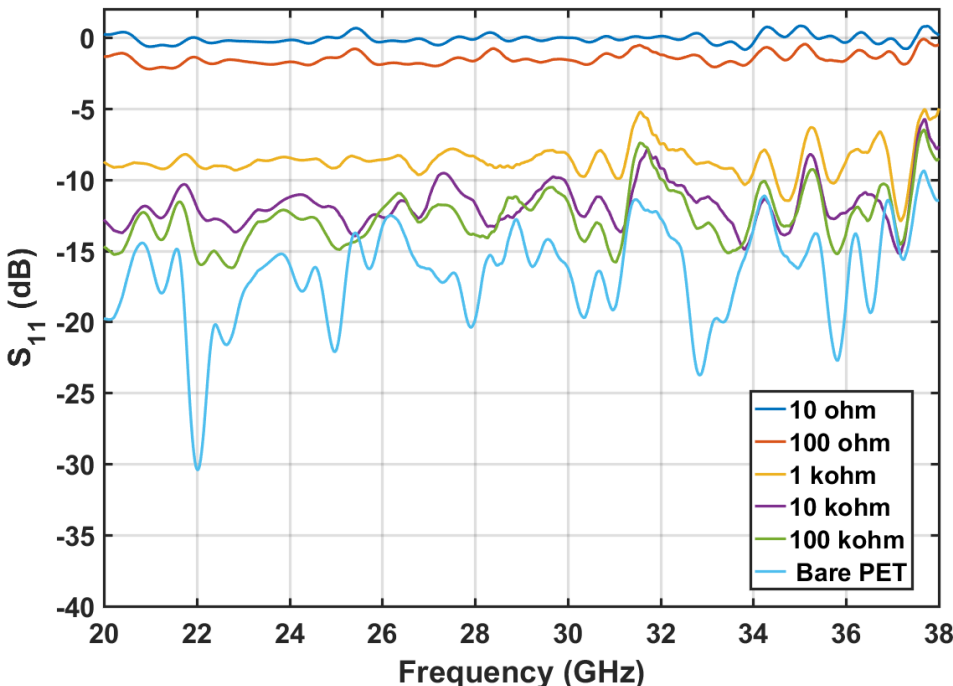
Figure 2. 17 Reflectance (dB) values of Ag NW/PET samples.
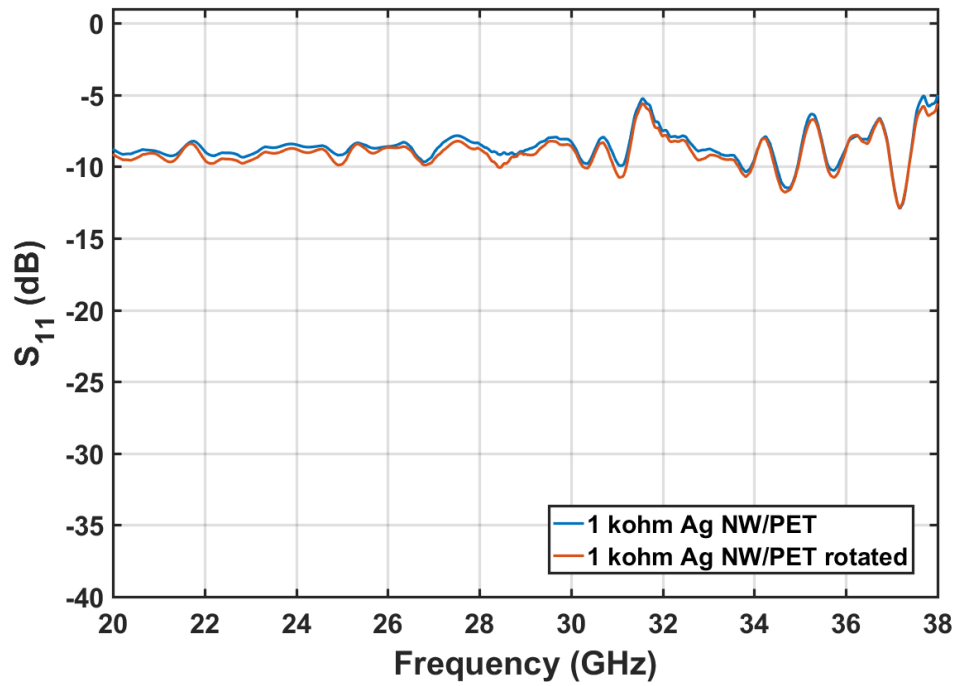
Figure 2. 18 Reflectance (dB) value of Ag NW/PET sample with a sheet resistance of 1 kohm before and after 90 degrees rotation.
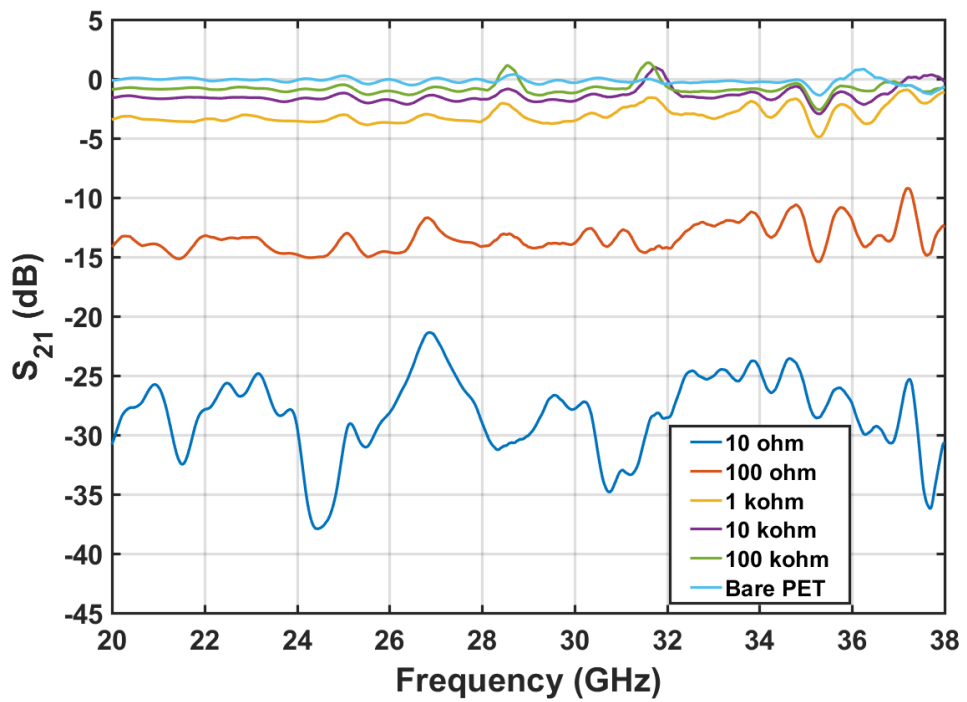
Figure 2. 19 Transmittance (dB) values of Ag NW/PET samples.

Apart from reflection and transmission values, percent absorption can be calculated using Equation 2.10. Absorbance graph thus obtained is provided in Figure 2.20. It is clear that the Ag NW/ PET sample with 1 kohm resistance absorbed 40 % of the incident wave and this was the highest value obtained among prepared samples.
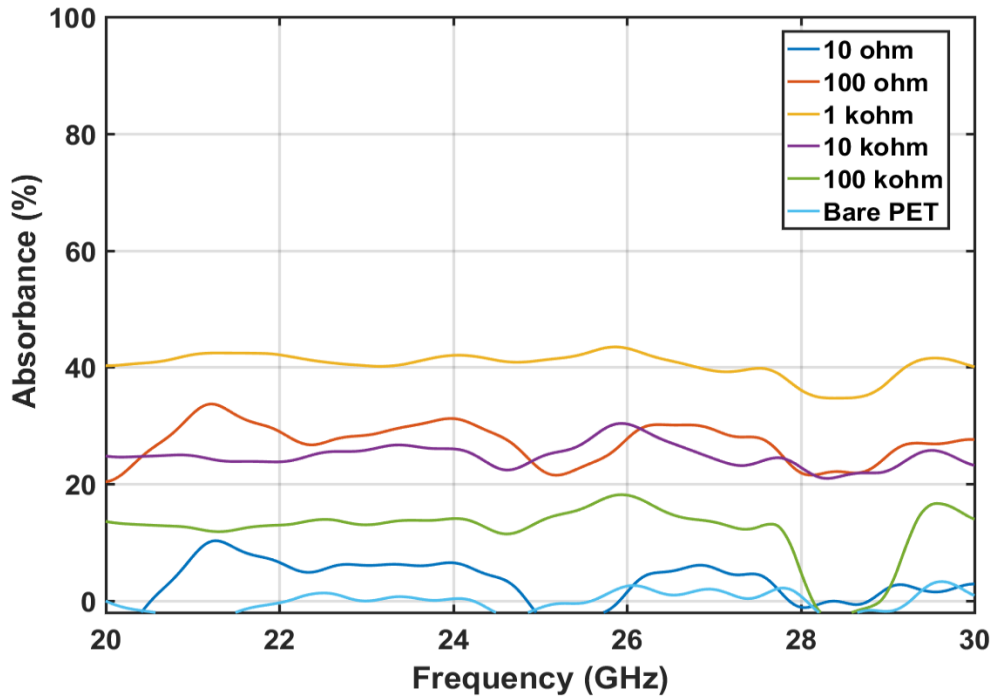
Figure 2. 20 Absorbance values of Ag NW/PET samples.

Upon considering all the transmission, reflection and absorption graphs, reflection dominant shielding was obtained with samples having 10 ohm and 100 ohm sheet resistance. For the sample having 10 ohm sheet resistance, approximately only 0.10 % of the incident wave was transmitted inside and for the sample having 100 ohm resistance approximately 3 % was transmitted. Moreover, investigation of absorption values revealed the potential of Ag NW/PET sample with 1 kohm sheet resistance to be used as an absorption dominant shielding material. This sample absorbed 40 % and reflected 10% of the incident wave. This means that 50 % of the wave was blocked and the remaining 50 % of the wave was transmitted. In order to minimize transmission, nickel (Ni) thin films with desired thickness were deposited through evaporation onto Ag NW networks.

2. 5. 2. 1. Nickel Evaporation onto Ag NW Networks on PET

5, 10 and 20 nm of Ni was deposited onto Ag NW networks on PET using a thermal evaporator at a base pressure of 1.5 x 10^{-6} Torr. In order to determine the effect of Ni thin films on Ag NW networks, Ni was first evaporated onto bare PET substrates. Optical transmittance of these samples with three different Ni thicknesses was measured by UV-VIS and the corresponding transmittance spectra is provided in Figure 2.21. It is clear from the transmittance results that the increased Ni thickness, decreased the transmittance of the substrates.
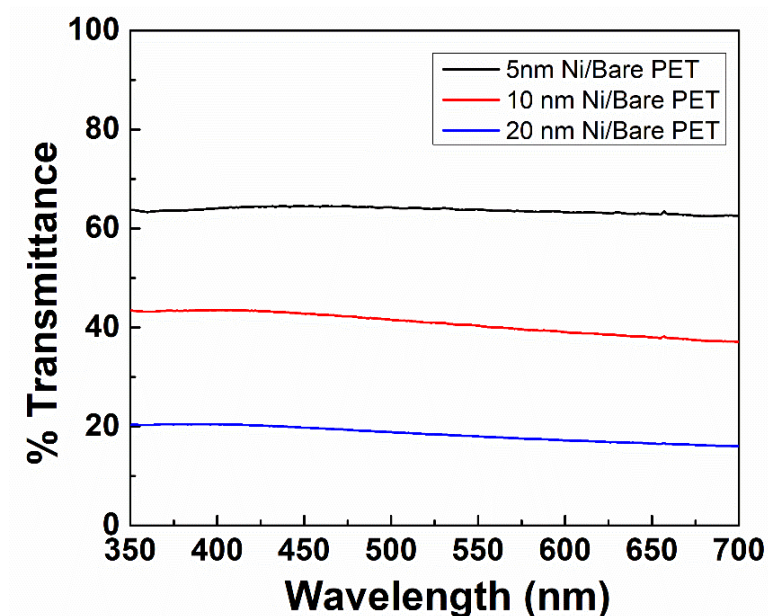
Figure 2. 21 Optical transmittance of Ni thin films on bare PET substrates.

EM measurements were made and obtained S_{11} values showed the reflectance (Figure 2. 22) and S_{21} values showed the transmittance of fabricated samples (Figure 2. 23). Transmittance and reflectance properties of the PET substrate can be changed according to the thickness of Ni. Ni thin films with 10 nm and 20 nm thickness showed

similar behavior to that of a bulk metal. However, Ni thin film with 5 nm thickness showed lower reflectance of approximately 25 % and a transmittance of 25 %.
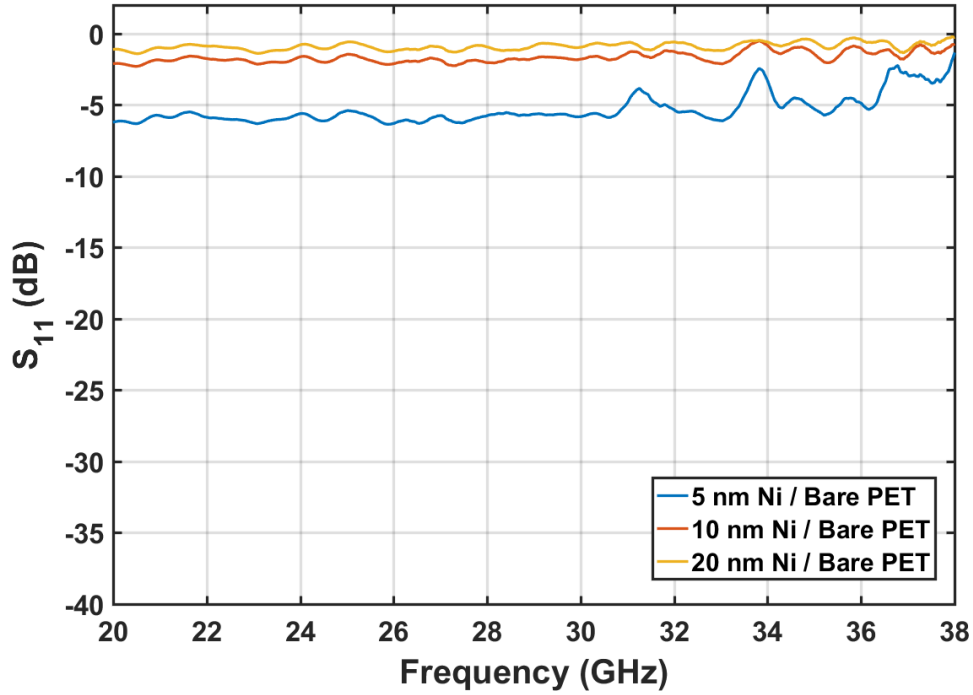
Figure 2. 22 Reflectance (dB) values of Ni/ PET samples.
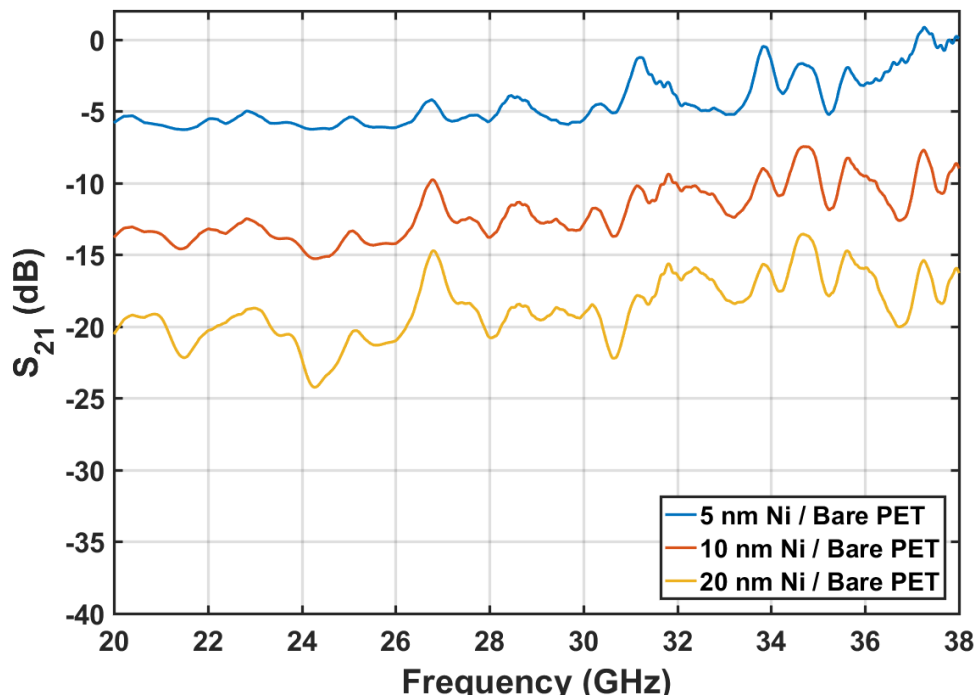
Figure 2. 23 Transmittance (dB) values of Ni/PET samples.

Percent absorbance values of the samples are provided in Figure 2.24. Highest absorption was observed for 5 nm thick Ni film. To clarify, 5 nm thick Ni film showed an average reflectance of 25 %, transmittance of 25 % and absorbance of 50 %. Thus, this surface modification method was found to be effectıve for the creation of absorption dominant shield materials. However, optical transmittance of this sample was lowered to 62 % as shown in Figure 2.21.
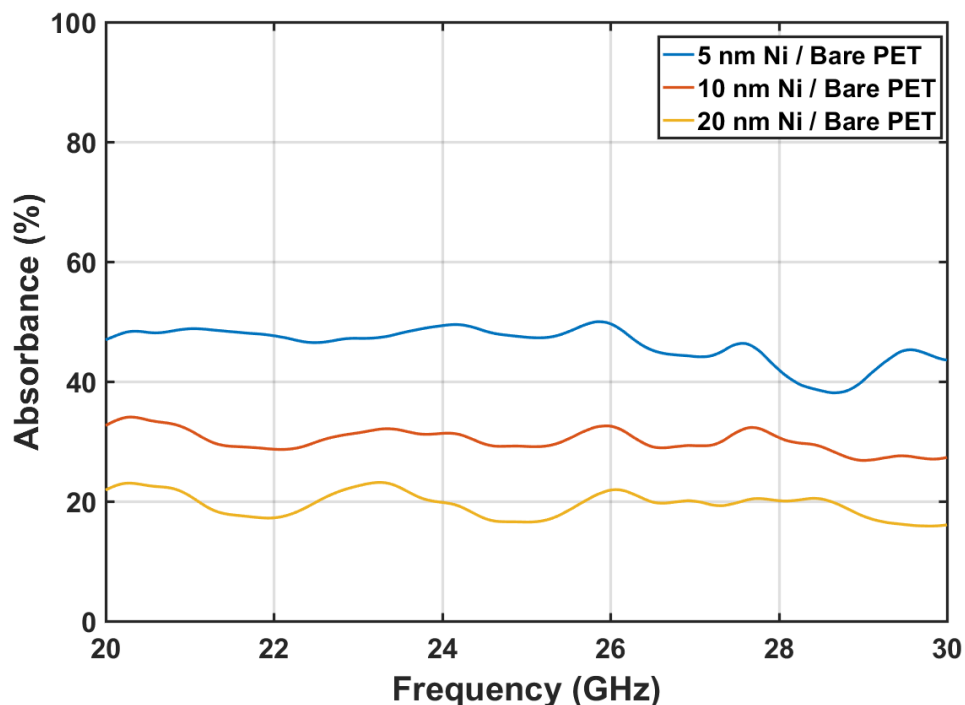
Figure 2. 24 Absorbance values of Ni thin films on bare PET substrates.

Following the characterization of Ni thin films on PET substrates, Ni thin films were deposited onto Ag NW networks on PET substrates. From the previous section, sample with sheet resistance of 1 kohm was selected considering its high absorbance. This sample was particularly chosen to improve and thus Ni deposition was made to obtain an absorption dominant shielding. Optical transmittance plot for Ni deposited Ag NW network with a sheet resistance of 1 kohm is provided in Figure 2.25. Transmittance values at a reference wavelength of 550 nm were found as 59, 35 and 14% for 5, 10 and 20 nm Ni deposited Ag NW networks on PET, respectively.
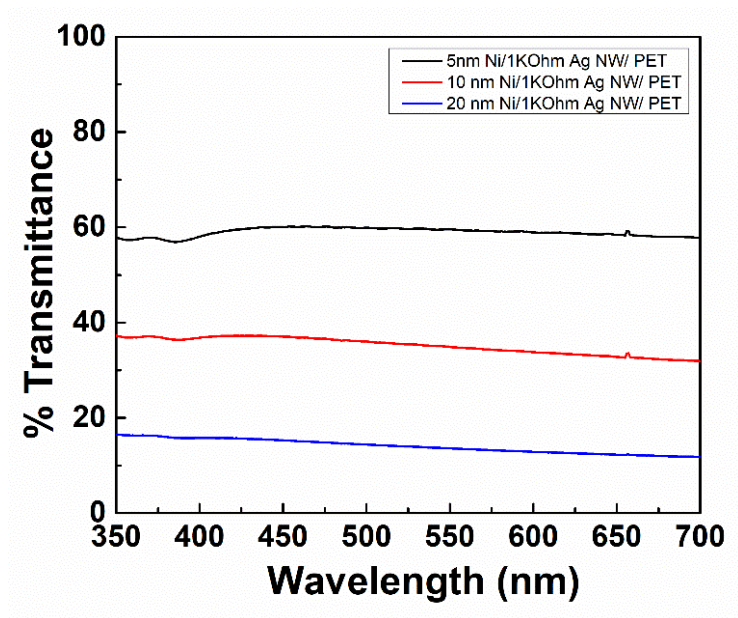
Figure 2. 25 Optical transmittance of Ni deposited Ag NW network with a sheet resistance of 1 kohm.

Moreover, SEM analysis was carried out for these samples to monitor the morphological changes upon Ni deposition. SEM images of 5, 10 and 20 nm thick Ni evaporated Ag NW network with a sheet resistance of 1 kohm are provided in Figure 2.26 (a)-(c), respectively. However, no discernable features were observed in SEM images. Thin film deposition was found to be highly homogeneous over the entire nanowire network.
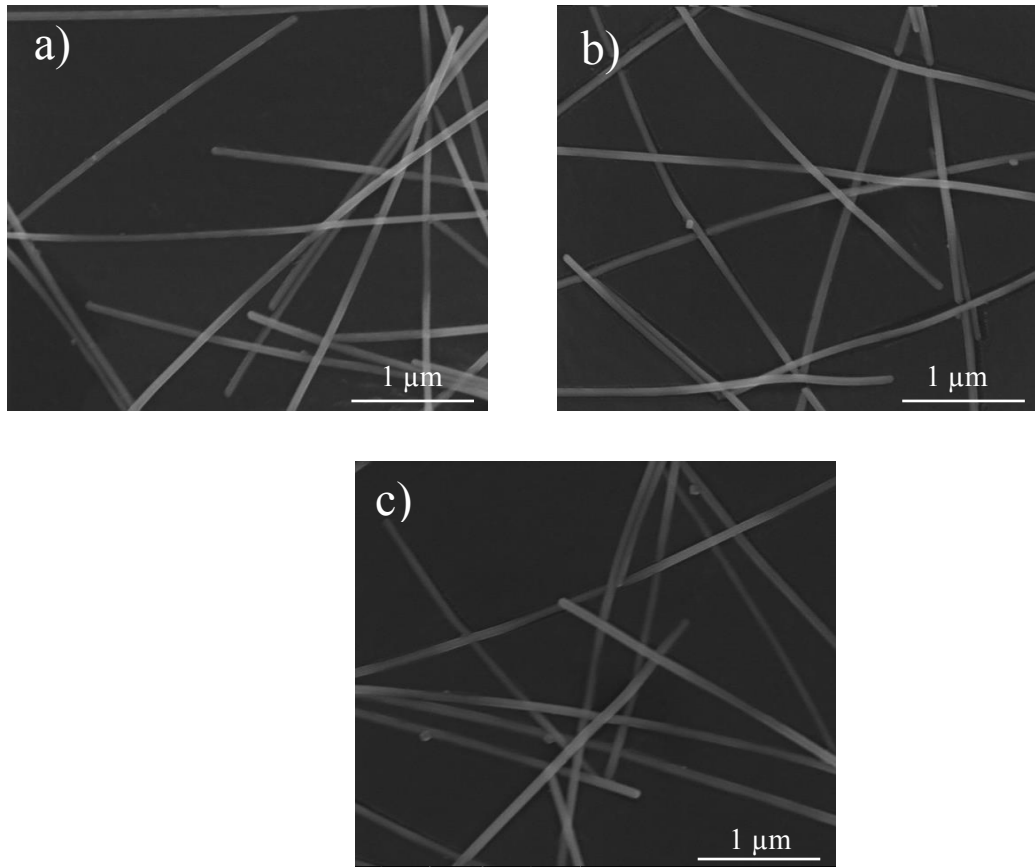
Figure 2. 26 SEM images of (a) 5, (b) 10 and (c) 20 nm thick Ni evaporated Ag NW networks with a sheet resistance of 1 kohm.

Results from EM measurements in terms of S_{11} values showing the reflectance and S_{21} values showing the transmittance values are provided in Figure 2.27 and 2.28, respectively. Deposition of Ni thin films onto Ag NW/PET samples clearly changed the transmittance and reflectance behavior and this change was found to be thickness dependent. Reflectance was found to increase, while the transmittance was found to decrease with increasing Ni thickness.
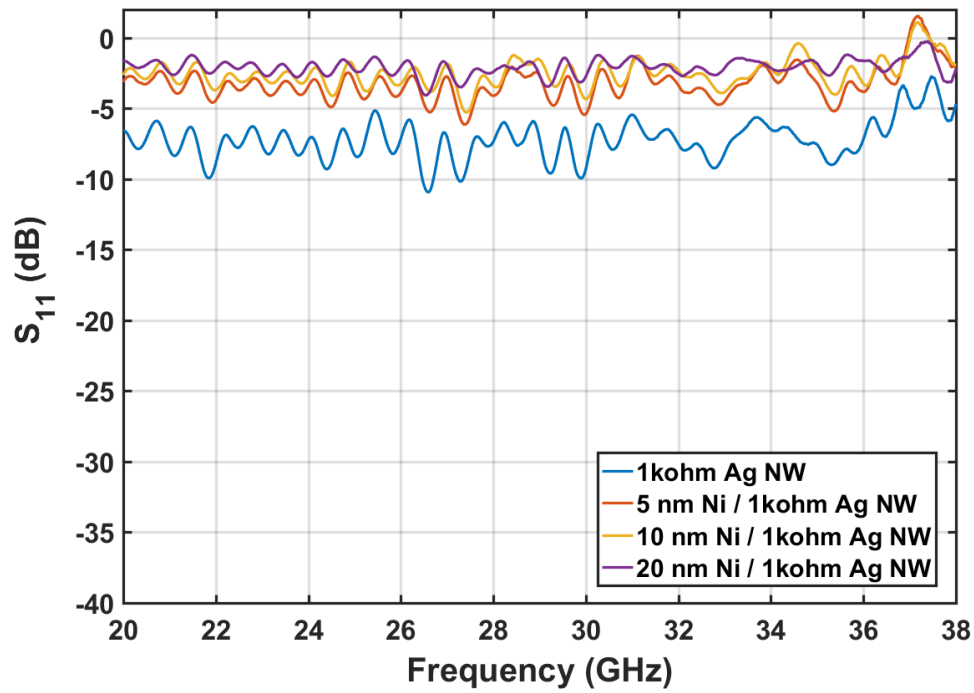
Figure 2. 27 Reflectance (dB) values of Ni/Ag NW/PET samples.
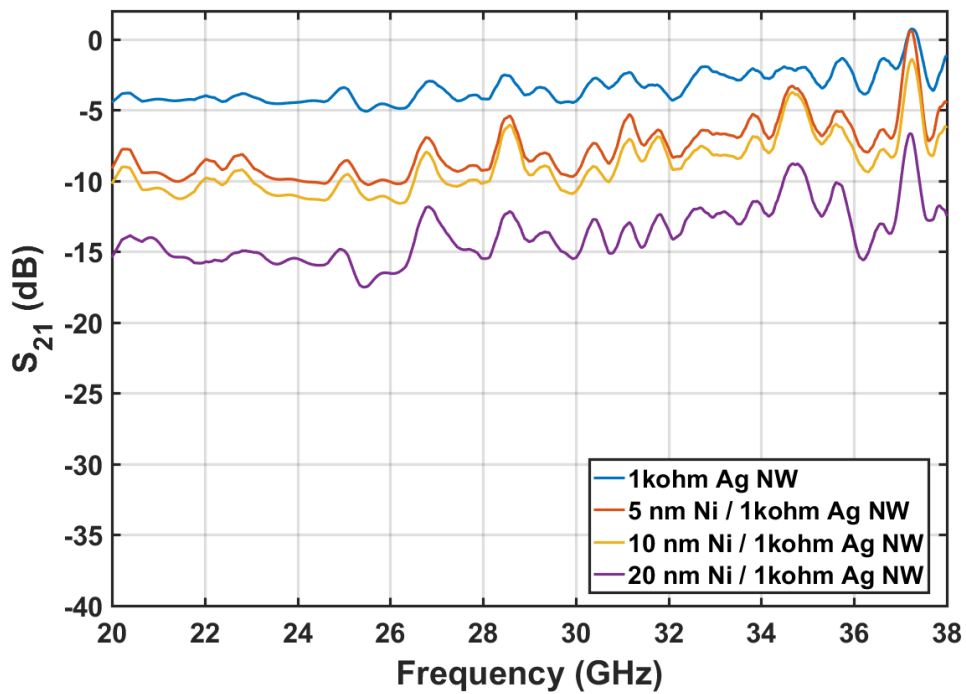
Figure 2. 28 Transmittance (dB) values of Ni/Ag NW/PET samples.

Absorbance values of the samples were calculated and the results are provided in Figure 2.29. A frequency dependent absorption increase was obtained. In order to clarify reflectance, transmittance and absorbance values of the samples at a frequency of 26.8 GHz were tabulated and provided in Table 2.3. This frequency was selected because it is the geometric mean of 18 - 40 GHz range and secondly because the lenses were designed according to this frequency.
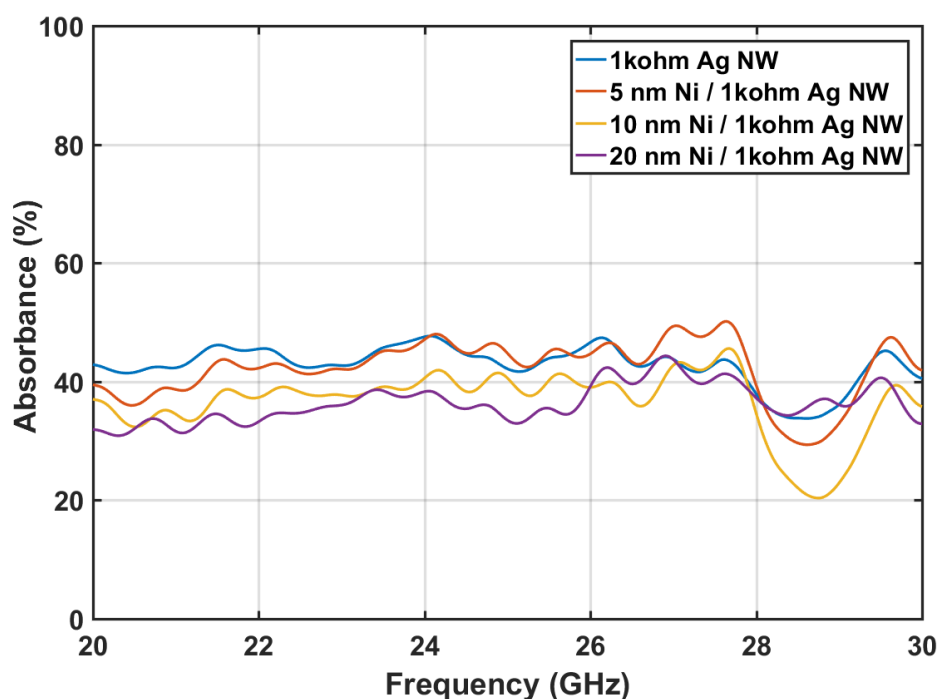
Figure 2. 29 Percent absorbance values of Ni/ Ag NW/ PET samples.

Table 2 3. EM measurement results of the samples at a frequency of 26.8 GHz.

	Reflectance (dB)	Transmittance (dB)	Absorbance (%)
5 nm Ni/ Ag NW/ PET	-4.214	-6.941	46.21
10 nm Ni/ Ag NW/ PET	-3.173	-8.004	38.38
20 nm Ni/ Ag NW/ PET	-2.278	-11.85	43.47
Ag NW/ PET	-8.326	-2.978	43.21

To sum up, through Ni evaporation, the shielding efficiency of Ag NW networks were improved. Evaporation of Ni increased the reflectance loss of the EM wave. However, optical transmittance values of the samples were significantly lowered upon Ni evaporation.

2. 5. 3. Silver Nanowire Networks on Textile

For this part of the thesis, a cotton textile was chosen as a substrate for the deposition of Ag NWs. Textile has been chosen as substrate since it has very wide application areas. In addition, smart textiles have a great potential in the market. Therefore, imparting EM shielding property to textiles through industrially viable and simple methods is highly promising.

Dip coating method was used for the decoration of Ag NWs onto textile substrates. Dip coating is one of the simplest and the most efficient coating methods, which is also readily practiced in industry. By this coating method, textile substrates were three dimensionally (3D) decorated with Ag NWs, which is critical for the investigation of their shielding efficiency behavior. SEM images of textiles prior to and after Ag NW decoration are provided in Figure 2.30 (a) and (b), respectively. Figure 2.30 (b) shows percolating and 3D decorated Ag NWs on textile fibers.
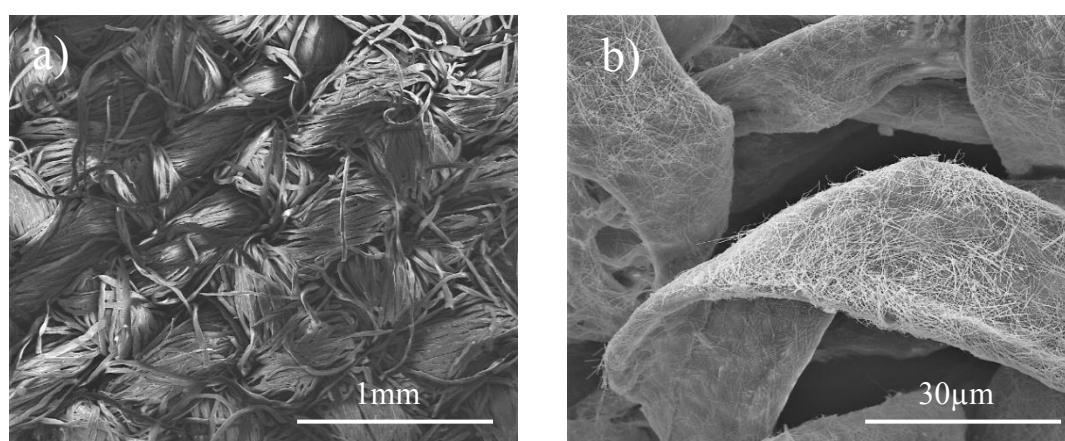
Figure 2. 30 SEM images of (a) bare textile and (b) Ag NW decorated textile with a resistance of 100 ohm.

Results obtained from EM measurements of the Ag NW decorated textile samples in terms of reflectance and transmittance are provided in Figure 2.31 and 2.32, respectively. Results obtained from bare textiles were also included in these graphs for comparison. While the reflectance from bare textiles were not prominent, decoration of Ag NWs onto the textile generated a conductive surface and 63 % of the incident wave was found to be reflected for the sample with 1 kohm resistance. On the other hand, transmittance of the samples was found to decrease to 5 % at a resistance of 100 ohm.
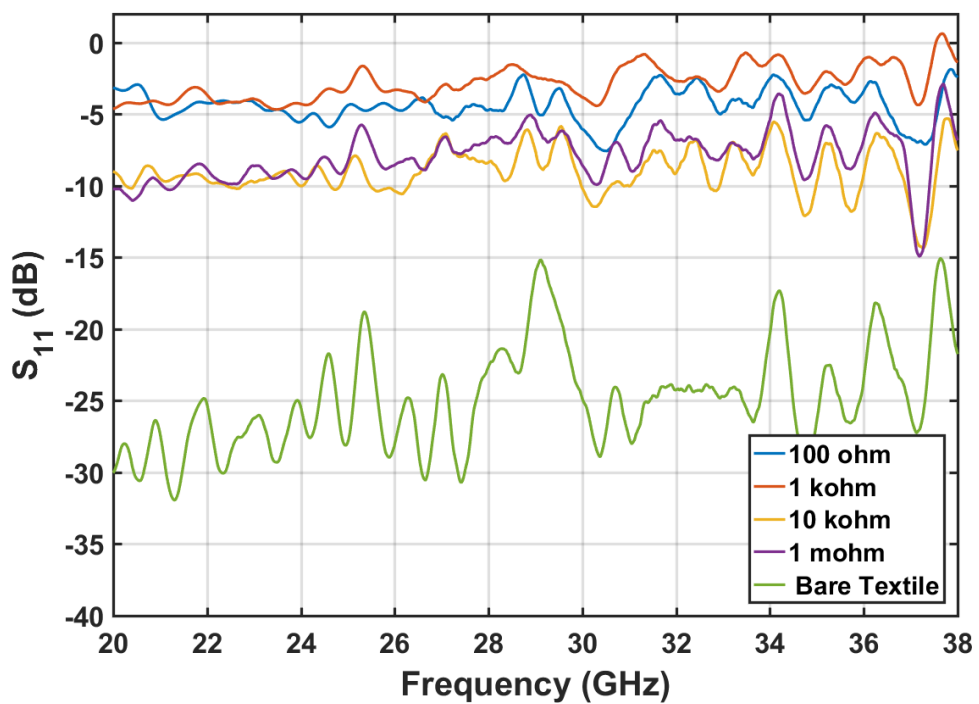
Figure 2. 31 Reflectance (dB) values of Ag NW decorated textiles.
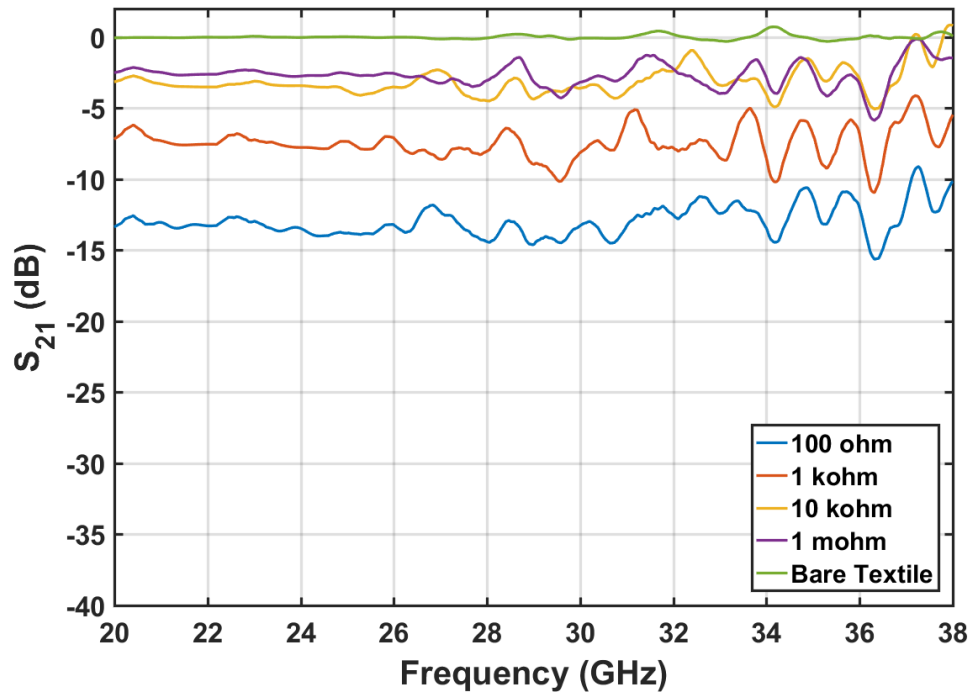
Figure 2. 32 Transmittance (dB) values of Ag NW decorated textiles.

Absorbance values of the samples were then calculated using reflectance and transmittance of the samples and the results are provided in Figure 2. 33. Among all samples investigated, the one with a resistance of 100 ohm showed the best shielding performance, which reflected 30 % of the incident wave while absorbing 65% of it. It showed an absorption dominant shielding. Only 5 % of the incident wave was transmitted. 3D nature of the textile was responsible for this efficient shielding.
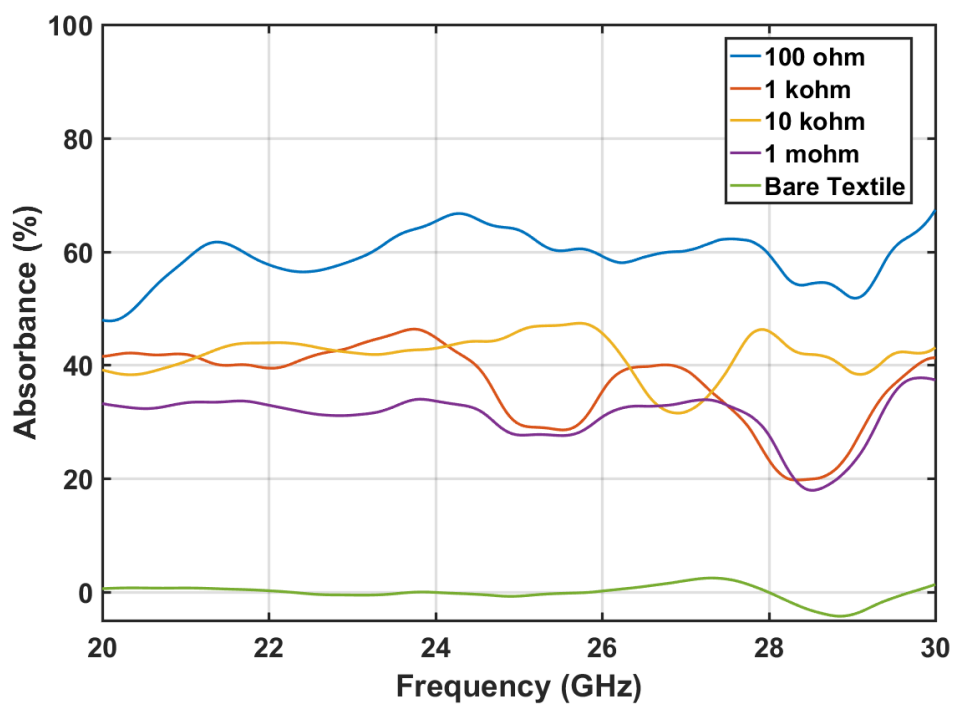
Figure 2. 33 Percent absorbance values of Ag NW decorated textiles.

In order to clarify the results, reflectance, transmittance and absorbance values of the samples at a frequency of 26.8 GHz were tabulated and presented in Table 2.4.

Table 2 4. EM measurement results of textile samples at a frequency of 26.8 GHz.

	Reflectance (dB)	Transmittance (dB)	Absorbance (%)
Bare Textile	-27.93	-0.11	2.34
100 ohm Textile	-4.41	-11.85	57.24
1 kohm Textile	-3.76	-8.25	40.01
10 kohm Textile	-7.79	-2.41	31.81
1 mohm Textile	-7.79	-3.08	32.93

It was found that the measurement direction of the textile samples affects the reflection and transmission characteristics. This was due to anisotropic nature of the textile originated from the knitting. Totally different values were obtained upon 90 degrees rotation of the sample. Effect of rotation on reflectance values can be observed in Figure 2.34. A maximum difference of 3 dB was measured between the two measurements, which was quite significant considering the logarithmic scale.
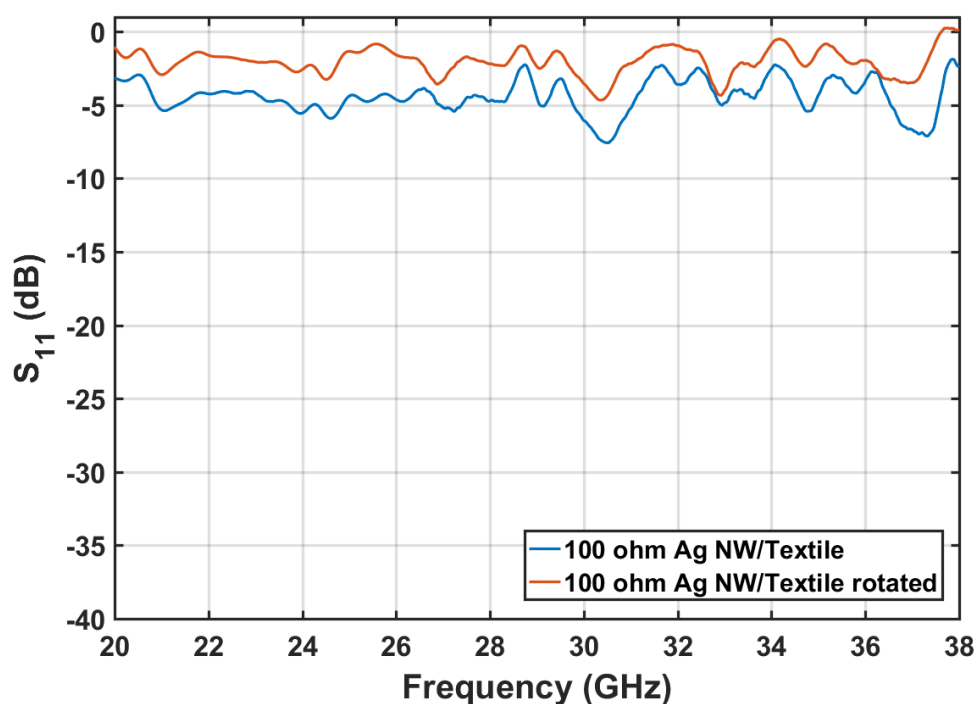
Figure 2. 34 Reflectance (dB) value of Ag NW decorated textile samples with a 100 ohm resistance before and after 90 degrees rotation.

2. 5. 4. Silver Nanowire Networks on Filter Paper

Filter paper was selected as another 3D substrate with random porosity. Through the use of this 3D structure, absorption capability of the samples can be highly improved. SEM images of filter papers prior to and following Ag NW deposition are provided in Figure 2. 35 (a) and (b), respectively.
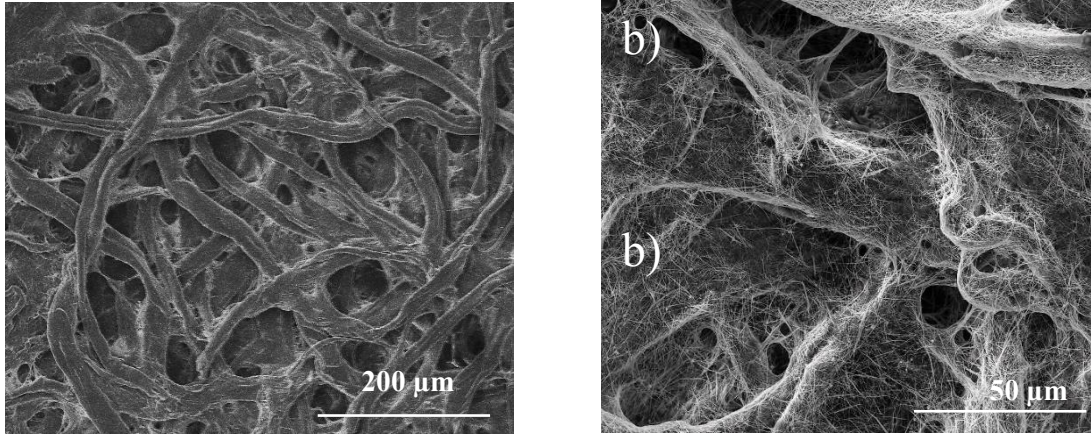
Figure 2. 35 SEM images of (a) bare filter paper and (b) Ag NW decorated filter paper with resistance of 100 ohm.

Results obtained from EM measurements of the Ag NW decorated. Filter papers in terms of reflectance and transmittance are provided in Figure 2. 36 and 2. 37, respectively. Results obtained from bare filter paper were also included in these graphs for comparison. While the reflectance from the bare filter paper were not prominent, deposition of Ag NWs onto the filter paper generated a conductive surface ad this time 80 % of the incident EM wave was found to be reflected for a sample with 10 ohm resistance. Furthermore, transmittance of the samples was found to decrease to 0.1-0.3%. These results clearly showed that a reflectance dominant shielding material was obtained due to increased internal reflections made possible by the pores within the filter paper.
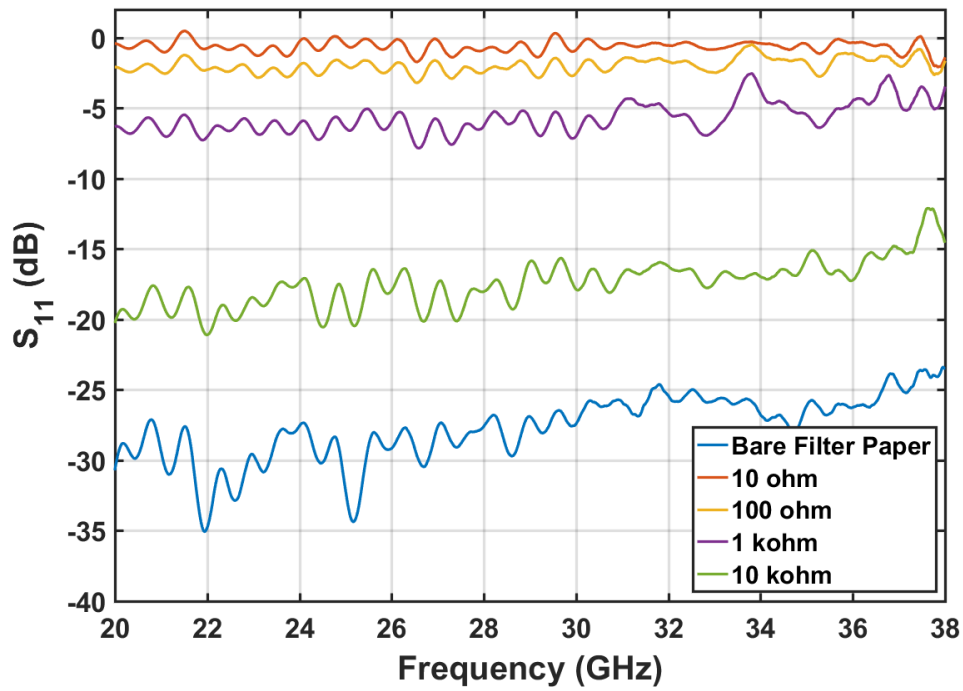
Figure 2. 36 Reflectance (dB) values of Ag NW deposited filter paper.
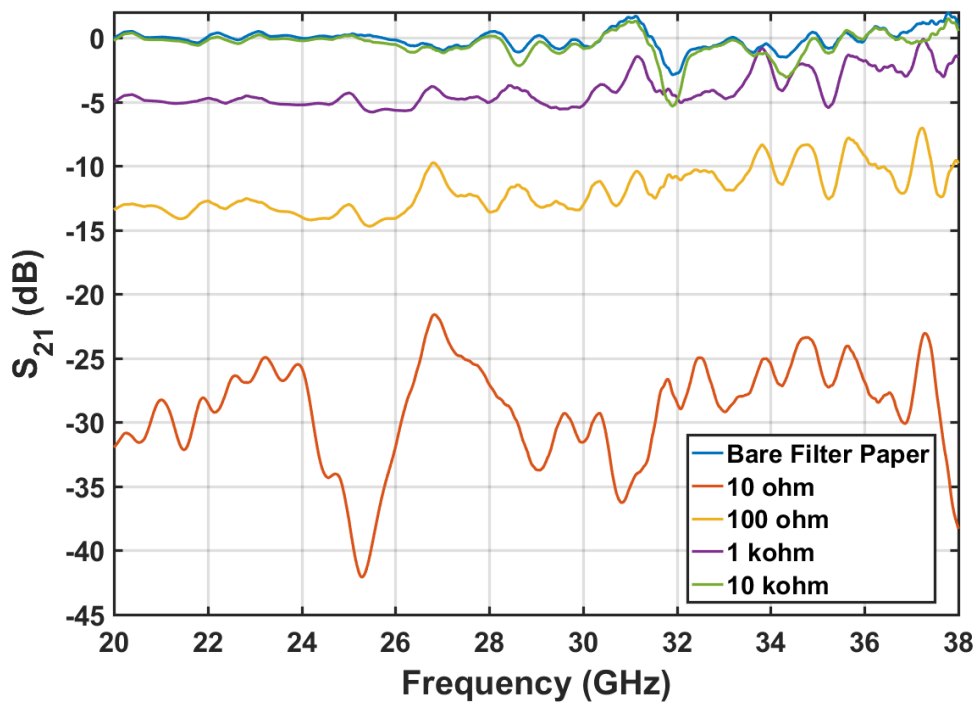
Figure 2. 19 Transmittance (dB) values of Ag NW deposited filter paper.

Absorbance values of the samples were calculated within a frequency range of 20-30 GHz and are provided in Figure 2. 38. The most absorbent sample was the one with a resistance of 1 kohm, which absorbed 40-42 % of the EM wave. Reflectance of this sample was 19-25 % (Figure 2. 36). Next, the obtained characteristics of filter paper and PET samples with a resistance of 1 kohm are compared and an approximately 10-15 % decrease in transmittance was observed. This decrease was attributed to the porous nature of the filter paper, which was responsible for the depletion of EM wave within the filter paper. Substrate change enhanced the shielding behavior by increasing absorption and reflection approximately by 5 and 10% respectively. Thus, the substrate selection was found to be highly critical in determining the EM wave interaction characteristics.
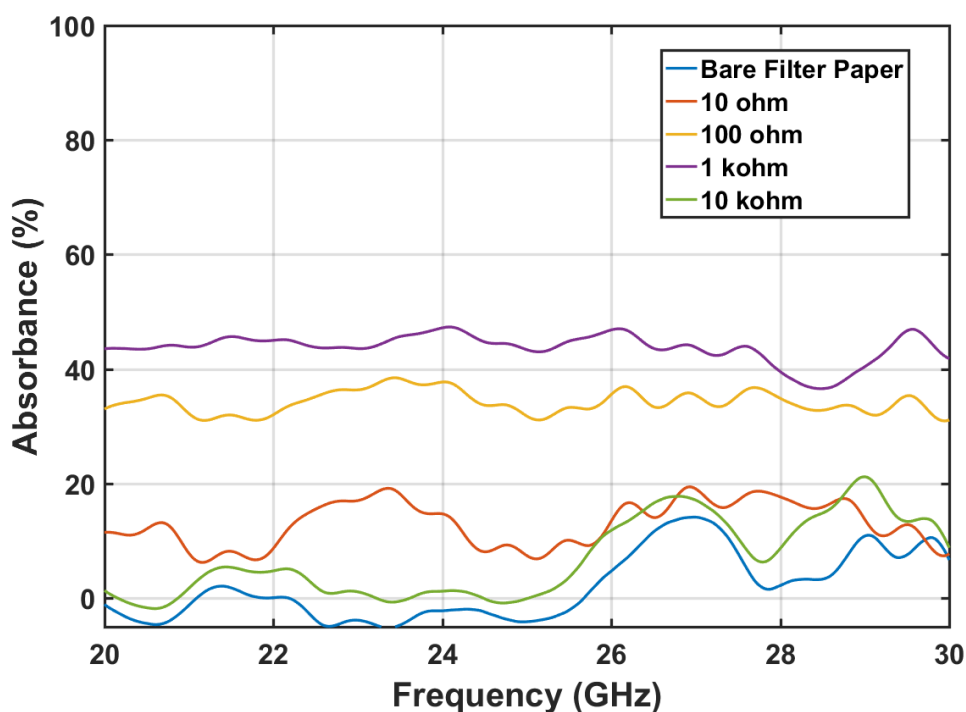
Figure 2. 38 Percent absorbance values of Ag NW deposited filter paper.

To summarize the results, EM reflectance, absorbance and transmittance of for Ag NW deposited filter papers with different resistances at a frequency of 26.8 GHz were tabulated and presented in Table 2. 5.

Table 2 5. EM measurement results of Ag NW deposited filter papers at a frequency of 26.8 GHz.

	Reflectance (dB)	Transmittance (dB)	Absorbance (%)
Bare Filter Paper	-29.78	-0.88	13.92
10 ohm Filter Paper	-0.5139	-21.61	18.23
100 ohm Filter Paper	-2.209	-9.758	35.26
1 kohm Filter Paper	-6.406	-3.81	44
10 kohm Filter Paper	-19.47	-0.8894	18.23

2. 5. 5. Silver Nanowire Networks on Felt

For this part of the thesis, felt was chosen as another substrate. Felt is a kind of textile made by rolling and pressing wool or fibers. It is mostly used as an isolation material. Therefore, integrating electromagnetic shielding into felt substrates is promising for applications simultaneously requiring thermal insulation and EM shielding.

Dip coating method was applied again for the decoration of Ag NWs onto felt. SEM images of felts prior to and following Ag NW decoration are provided in Figures 2.30 (a) and (b), respectively. Figure 2.39 (b) shows percolating and 3D decorated Ag NWs on felt fibers.
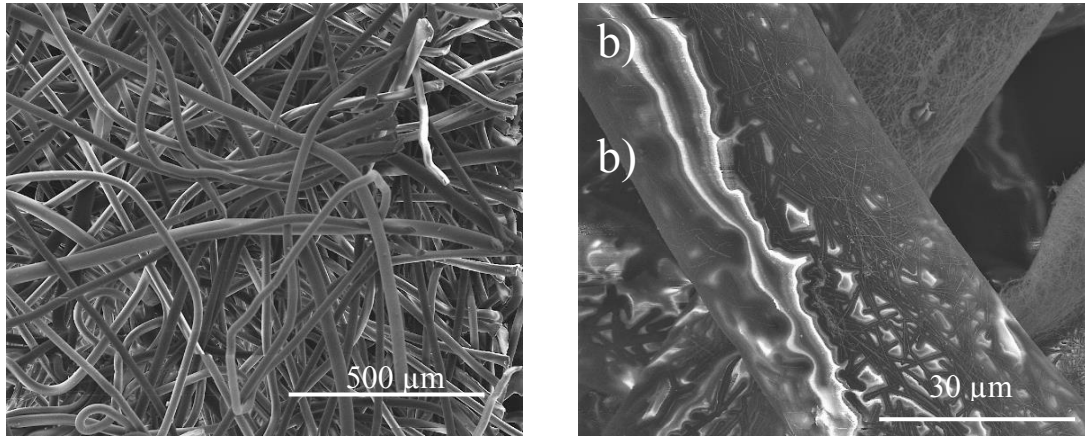
Figure 2. 39 SEM images of (a) bare and (b) Ag NW decorated felt with a resistance of 100 ohm.

EM wave reflectance and transmittance characteristics of the Ag NW decorated felts are provided in Figure 2. 40 and 2. 41, respectively. Reflectance of the EM wave was found to increase with a decrease in the resistance of the samples. A maximum reflectance value of 60 % was obtained from the sample with 100 ohm resistance. It was observed from Figure 2.41 that the transmittance of the incident wave was 2%.
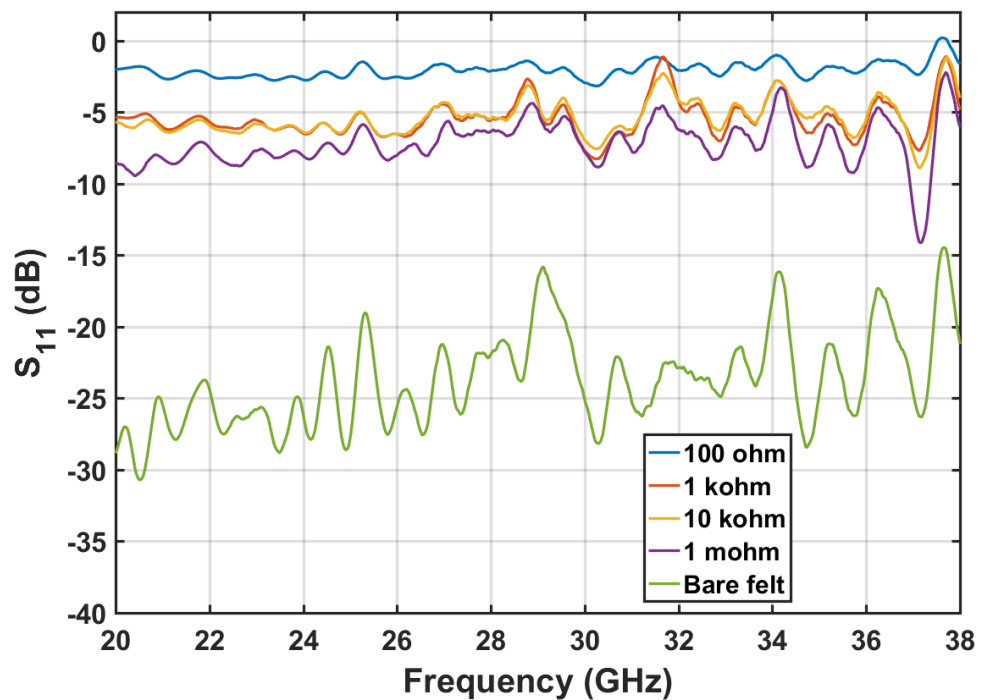
Figure 2. 40 Reflectance (dB) values of Ag NW decorated felt
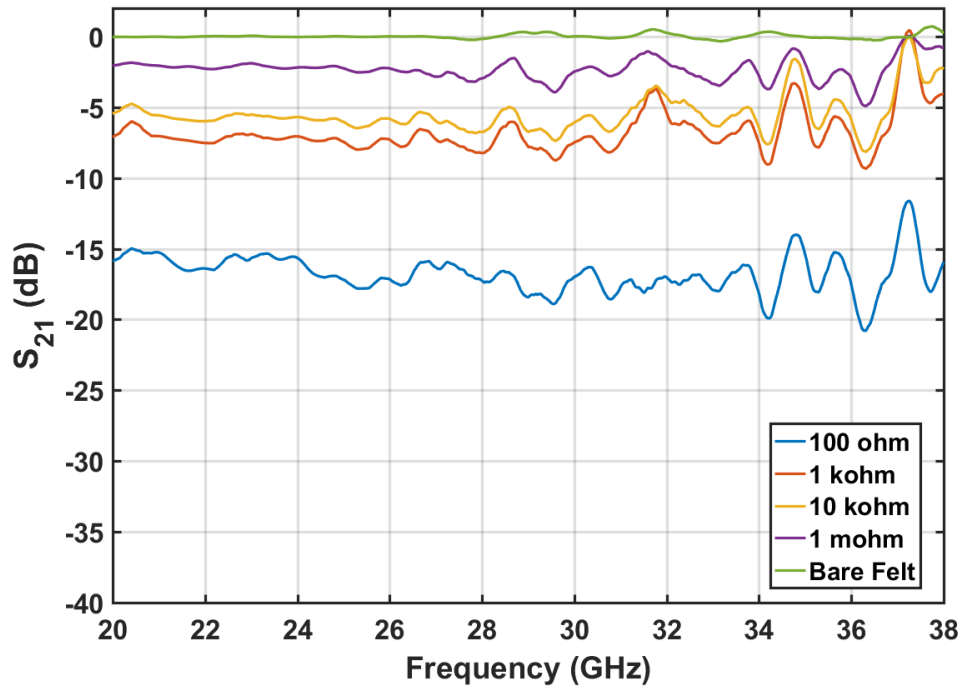
Figure 2. 41Transmittance (dB) values of Ag NW decorated felt.

While reflectance dominant shielding was observed from the sample with a resistance of 100 ohm, absorbance dominant shielding potential was observed from the sample with a resistance of 1 kohm. Absorbance values of the samples are provided in Figure 2.42 and this sample was found to show the highest absorption of up to 60 %. However, approximately 20 % of the wave was found to transmit through the material, which should not be ignored. Reflectance, transmittance and absorbance values of the Ag NW decorated felts at a frequency of 26.8 GHz were tabulated and provided for comparison in Table 2.6.

52

Table 2 6. EM measurement results of felt samples at a frequency of 26.8 GHz.

	Reflection (dB)	Transmission (dB)	Absorption (%)
Bare Felt	-22.99	0	0
100 ohm Felt	-2.588	-15.92	35.35
1 kohm Felt	-3.556	-6.659	44
10 kohm Felt	-4.54	-5.447	37
1 mohm Felt	-8.841	-2.663	24
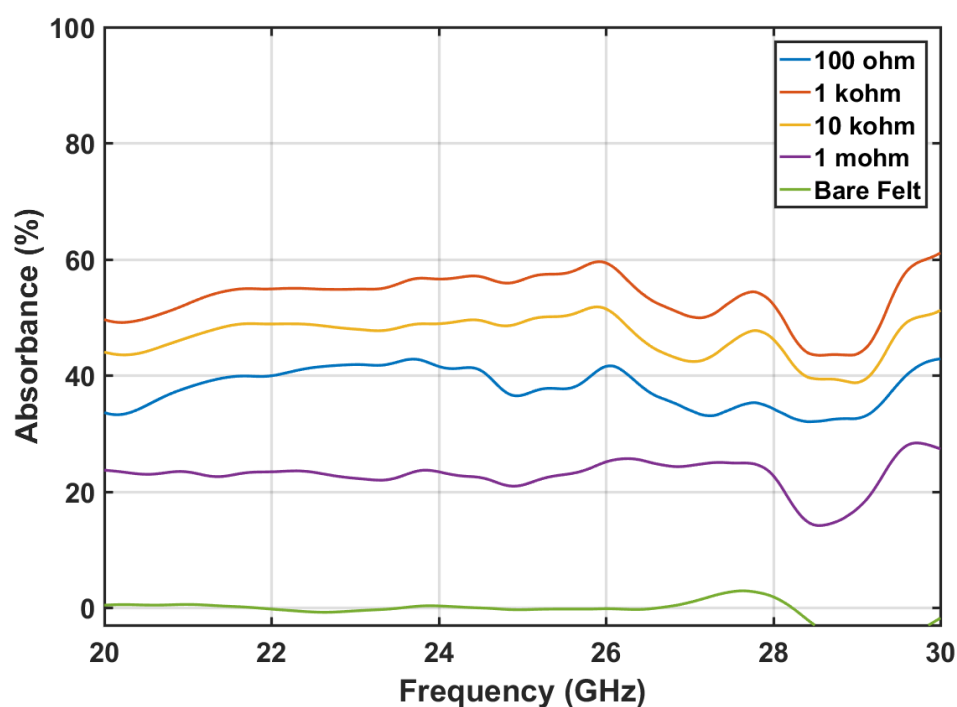
Figure 2. 42 Absorbance values of Ag NW decorated felt.

To sum up, non-conductive materials can be made electrically conducting upon decoration/deposition of Ag NWs using simple processes. For PET samples a 2D network of Ag NWs was obtained, whereas for the filter paper, felt and textile samples a 3D network of a Ag NW network was achieved. All the reflectance, transmittance and absorbance characteristics of the samples were tabulated for comparison and provided in Table 2. 7. Bare samples were found to transmit all of the incident EM wave. Decoration / deposition of Ag NWs significantly decreased the transmittance of the EM wave. A reflection dominant shielding was obtained for Ag NW decorated

cotton textiles and felt. Also, an absorption dominant shielding was observed for the textile samples. Among all samples, the lowest transmittance of 1% was observed for the Ag NW deposited filter paper with a resistance of 10 ohm. Shielding efficiency for this sample was obtained as -21.61 dB, which signifies almost 99 % shielding of the incident EM wave.

Table 2 7. EM measurement results at a frequency of 26.8 GHz.

Samples	Reflectance (dB)	Transmittance (dB)	Absorbance (%)
20 nm Ni / 1 kohm Ag NW/ PET	-2.278	-11.85	43.47
Ag NW/ PET	-8.326	-2.978	43.21
10 ohm Filter Paper	-0.5139	-21.61	18.23
Bare Filter Paper	-29.78	-0.88	13.92
100 ohm Textile	-4.41	-11.85	57.24
Bare Textile	-27.93	-0.11	2.34
100 ohm Felt	-2.588	-15.92	35.35
Bare Felt	-22.99	0	0

CHAPTER 3

SILVER NANOWIRES AS TRANSPARENT ELECTRODES FOR ORGANIC SOLAR CELLS

3. 1. INTRODUCTION

With the increase in population and development of the technology and industry, energy consumption increases steadily. Many countries use fossil fuels, such as coal, oil and natural gas as energy sources in order to meet their energy demand. Satisfying the energy need from those sources raises two problems that are the depletion of the source and green-house effect. Since these natural sources are limited, they can only be used until they are depleted. Moreover, since the dependence on fossil fuels are increasing, the amount of greenhouse gases released into the atmosphere increases significantly [35]. Solar radiation that is coming from the sun can be trapped at the atmosphere and will lead to a rise in Earth's temperature. In the long term, global warming will lead to serious drawbacks for mankind [36]. In order to decrease the dependence on fossil fuels, researchers are looking for alternative energy sources. The term 'green energy' is created to describe the energy sources, which are renewable and environmentally friendly. Geothermal energy, wind energy, wave energy and solar energy are the most feasible types of green energy [37].

Solar energy has a great potential considering the energy demand of the earth. The solar energy received in less than an hour can easily fulfill the worlds annual energy demand [38]. In order to use this energy efficiently, scientists are working on the development of various types of solar cells. Solar cells simply convert solar energy into electricity. Inorganic semiconductor materials are used firstly in solar cell applications. These are silicon (Si), cadmium telluride (CdTe), copper indium gallium diselenide (CIGS). The reason why these materials are selected for the fabrication of

solar cells is their suitable band gaps, availability and cost. They have band gap values between 1.1 and 1.7 eV, which is close to the optimum level (1.5 eV) [39]. However, these solar cells are not flexible and are not sustainable due to limited availability of the inorganic materials. On the other hand, organic solar cells (OSCs) are seen as the next generation of the photovoltaics. They are cheaper than the inorganic counterparts. They can be easily processed by solution-based methods unlike inorganic solar cells. They are flexible and thus can be fabricated by roll-to-roll production methods. Polymers are readily available with a wide range of parameters and the organic solar cells are potentially disposable. Therefore, organic solar cells are environmentally friendly. In addition, novel concepts such as semi-transparent organic solar cells can be fabricated, which opens up many application areas, such as building integrated photovoltaics. However, organic solar cells have lower power conversion efficiencies when compared to inorganic based counterparts. Moreover, they have lower lifetime [40].

In this thesis to replace indium thin oxide (ITO), Ag NW networks are integrated as transparent electrodes for organic solar cells. Firstly, the spray coated, conductive and transparent Ag NW network is used as the bottom electrode in order to replace commercial standard ITO in solar cell architecture. Secondly, Ag NW networks fabricated on polydimethylsiloxane (PDMS) substrates are used as the top contacts in inverted organic solar cells to replace evaporated metals.

3. 2. THEORY AND LITERATURE REVIEW

3. 2. 1. Operation Principle of Solar Cells

Operation of solar cells are based on the photovoltaic effect. It was found by Edmond Becquerel in 1839. It is the light dependent generation of a voltage in a photovoltaic cell. Firstly, the material should absorb photons. When the energy of the photon is larger than the band gap of the material, it absorbs this energy. With this energy, electrons are raised to higher energy states and move among the external circuit. Electrons return to solar cell, when all the energy is dissipated. pn semiconductor junctions are desired for this application. *n*-type semiconductors have larger electron density, lower hole density, whereas *p*-type semiconductors have larger hole density and lower electron density. As it is also shown in Figure 3.1, solar energy is converted into electrical energy in four steps. These are

- Absorption of light and creation of electron-hole pairs (exciton),
- Diffusion of exciton to an interface,
- Separation of an exciton into individual electrons and holes
- Charge transport (holes to anode, electrons to cathode) and eventually collection [40].
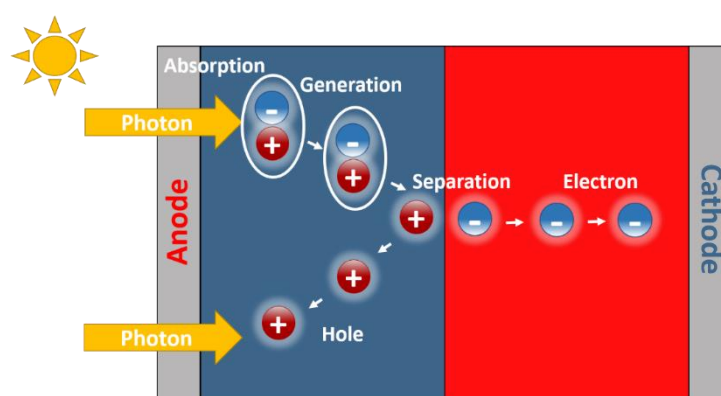
Figure 3. 2 Schematic showing the operation principles of OSCs.

3. 2. 2. Types of Organic Solar Cells

Three types of OSCs are present in the literature. These are single layer OSCs, bilayer OSCs and bulk heterojunction OSCs.

Single layer organic solar cells

This structure is introduced first. In this structure, single organic layer is evaporated between two metal electrodes having different work functions. This difference in the work function generates an electric field in the conducting organic layer, when connected to an external circuit. Electric field in the organic layer breaks up the electron-hole pairs (excitons). Electrons are excited to LUMO level (lowest unoccupied molecular orbital also known as conduction band), whereas holes remain on the HOMO level (highest occupied molecular orbital also known as valence band). Then, electrons are pulled towards the cathode (+ electrode) and holes are pulled towards the anode (- electrode). For charge generation, single layer devices should have a Scottky barrier at either of the contract. By this barrier, depletion region can be formed at the semiconductor/metal interface, which allows the separation of excitons as shown in Figure 3.2. However, exciton formation and separation are only limited to this small region as a disadvantage of this device structure [40].
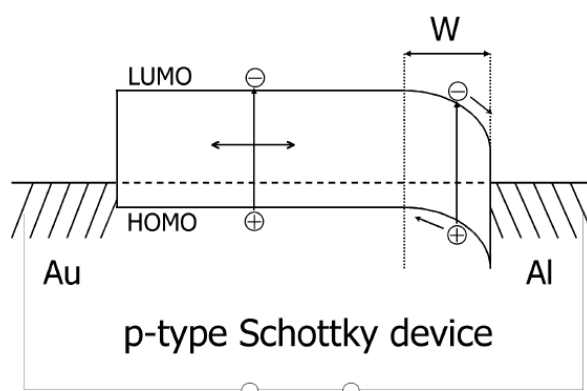
Figure 3. 5 A schematic structure of single layer OSC with a Schottky contact near Al electrode [40].

Although single layer OSCs have a simple fabrication route, there are a few other drawbacks associated with this structure. This kind of organic photovoltaics have low quantum efficiency and conversion efficiency due to the fact that electron and hole recombination is highly probable, since these both carriers have to travel in a single organic layer.

Bilayer organic solar cells

In bilayer OSCs, two semiconducting polymer thin films are deposited on top of each other. Layer with high electron affinity is called as the donor, while the other one is called as the acceptor. A large potential difference is required for charge separation. Separation of charges occurs at the planar interface between those two layers. Electrons travel within the acceptor (A), whereas holes travel within donor (D) layer as shown in Figure 3. 3 [40].
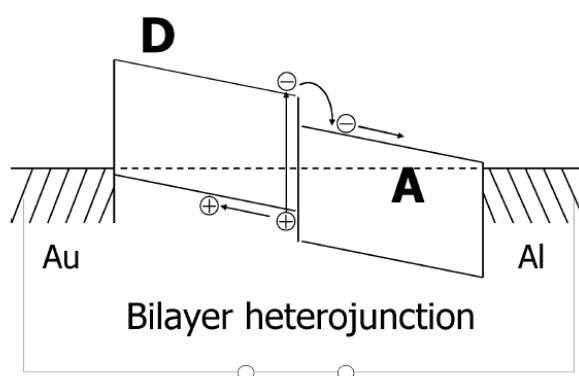
Figure 3. 8 Schematic structure of a bilayer OSCs [40].

In bilayer OSCs, the separation of the holes and electrons are more efficient and recombination is highly prevented when compared to single layer OSCs. There are still some problems that needs to be resolved. As only excitons that are generated only 10 nm apart from an interface gets dissociated, power conversion efficiency values are low.

Bulk heterojunction organic solar cells

Different from all structures, in bulk heterojunction OSCs, there is an active layer composed of the mixture of donor and acceptor polymers. As both components are

present in bulk volume, donor and acceptor interface is relatively large. Therefore, it is easier for excitons to dissociate.

In both bulk heterojunction and bilayer structures, there are acceptor and donor layers (Figure 3.4). However, due to large interfacial area at the bulk heterojunction, no loss is observed due to short diffusion distances. Excitons are ideally dissociated within their lifetime without recombination. Therefore, power conversion efficiencies are the highest among other OSCs. However, this blended bulk structure is sensitive to nanoscale morphology as percolation should be satisfied for both carriers [40].
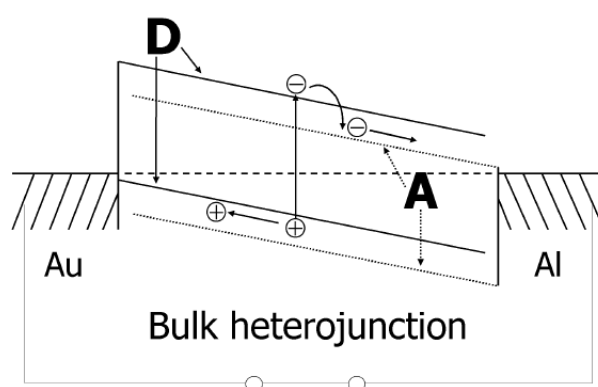
Figure 3. 9 Schematic structure of a bulk heterojunction OSC [40].

3. 2. 3. Inverted Organic Solar Cells

In previous section, types of OSCs were discussed. To sum up, in a typical OSC a semiconducting layer is placed between the anode and cathode as shown in Figure 3. 5 (a). For anode, commercially available ITO is preferred due to its high transparency and low sheet resistance. For hole injection layer typically, PEDOT: PSS is utilized. Al is selected as the cathode due to its low work function. Moreover, calcium (Ca= or lithium fluoride (LiF) is evaporated between the cathode and active layer as the electron injection layers. However, this architecture has several drawbacks. Main problem for this architecture is the stability. Low work function metals such as Al and Ca are selected as cathode materials, therefore, oxidation of the cathode is inevitable for this architecture [41]. Moreover, acidic nature of PEDOT: PSS can lead to device degradation by reacting with the active layer or by etching underlying ITO [42]. In

order to avoid these problems, device architecture is inverted as shown in Figure 3.5 (b). In inverted device structure, n-type semiconductors such as ZnO, TiO_x are placed over ITO for efficient electron collection. Then, active layer is deposited. Air stable metals such as Ag can be used as the top electrode and oxidation of top contact is prevented. In some structures, PEDOT: PSS is replaced with alternative hole transporting contacts (i.e. molybdenum oxide, MoO_3) and degradation from acidic nature of PEDOT: PSS is prevented. Inverted structures have much higher power conversion efficiencies as compared to conventional solar cell structure [43].
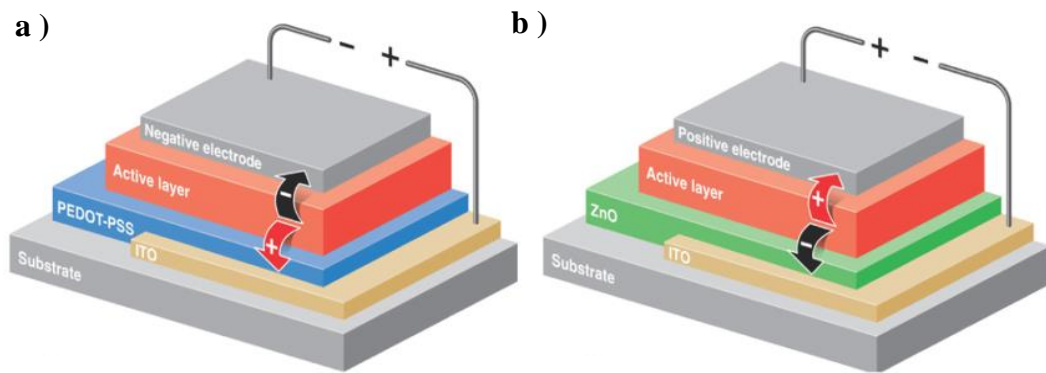
Figure 3. 11 Schematic structures of (a) conventional and, (b) inverted OSCs [43].

3. 2. 4. Solar Cell Characterization

Solar cells do not generate current until they are illuminated. Following illumination, device starts to generate power. Therefore, I-V curve of the device is shifted towards the fourth quadrant. There is a point over the curve at which both voltage and the current have their maximum values. This point is called as the maximum power point. V_{OC} is the open circuit voltage. It is the maximum voltage value attained, when the current is zero. I_{SC} is the short circuit current, which is the maximum current value attained, when the voltage is zero, as shown in Figure 3. 6 [40][44].
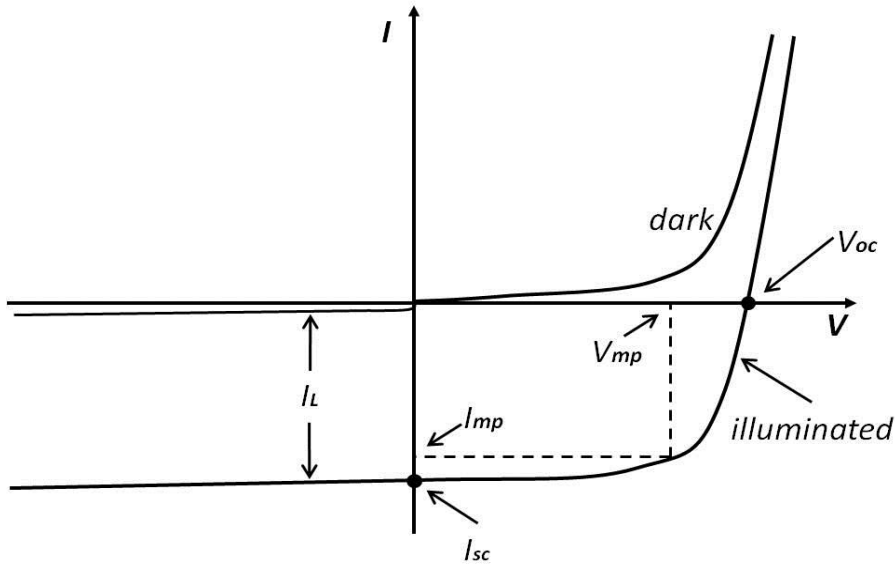
Figure 3. 12 Typical I-V curve of a solar cell both in dark and under illumination.[41]

In order to determine the efficiency of a solar cell, one more term needs to be defined, which is the fill factor (FF). Fill factor is the ratio between the rectangular area of maximum points and the rectangular area created by open circuit voltage and short circuit current. Equation 3.1 is used to calculate FF. Reasonable fill factor values lie between 0.7 and 0.85 [45].

$$FF = \frac{V_{MP} \times I_{MP}}{V_{OC} \times I_{SC}} \qquad (3.1)$$

Power conversion efficiency is then the ratio between the power obtained by the maximum points and the incident light power density, which is calculated in Equation 3.2. During all device characterizations, this light power density is standardized at 1000 W/m^2 with the AM 1.5 spectrum [46].

$$\eta_e = \frac{V_{MP} \times I_{MP}}{P_{in}} = \frac{V_{OC} \times I_{SC} \times FF}{P_{in}} \qquad (3.2)$$

Factors affecting Open Circuit Voltage: V_{OC} indicates the amount of recombination within the device. In organic photovoltaics, V_{OC} depends on the energy difference between HOMO level of donor and LUMO level of the acceptor [47]. In order to change this value, some modifications in the cell structure can be made. ITO can be modified by plasma etching or coated with a higher work function organic layer to

62

improve the matching between the energy levels of anode and HOMO of the hole conducting layer. Open circuit potential increases with the magnitude of band gap. Modification at the interface between metal and organic semiconductor affects the V_{OC} value and the work function of the electrodes. Therefore, oxide formation strongly changes the V_{OC}. For instance, it is often preferred to evaporate thin films of lithium fluoride (LiF) between anode electrode and the organic semiconductor to increase the V_{OC} value [48].

Factors affecting Short Circuit Current: It is assumed that the light generated current and I_{SC} are equal to each other when the device is ideal. According to this assumption, I_{SC} would be the largest current value obtained from the device. Basically, it depends on the charge carrier density and their mobility. An increase in the generation and the collection of light generated carriers increases the I_{SC}. Therefore, it strongly depends on the generation rate and diffusion length of the carriers.

Factors affecting Fill Factor
It is proportional to the amount of charge carriers that reach the electrode. Not all generated charge carriers are transported to the electrode, some of them are recombined. Lifetime and mobility of the carriers should be maximized in order to improve their diffusion length. Moreover, series resistance should be minimized and shunt resistance should be maximized to maximize FF [49][50].

3. 2. 5. Literature review

As it is mentioned before, transparent electrodes are very important in today's technology. Sputtered metal oxide thin films (i.e. indium tin oxide (ITO), fluorine doped tin oxide (FTO), aluminum doped zinc oxide AZO) are widely used as transparent electrodes [40]. They have sheet resistance values under 20 ohm /square at an optical transmittance of 90 % at a wavelength of 550 nm. One alternative for metal oxide thin films is Ag NW networks [51][52][53][54]. In fact, Ag NW networks are used as transparent electrodes for OSCs in many different ways.

The biggest problem for using Ag NW networks as bottom electrode in OSCs is the roughness of the networks, which leads to shunting or shorting. Gaynor et. al. suggested an easy way to minimize surface roughness by embedding Ag NWs into PEDOT:PSS [55]. Firstly, they drop-casted Ag NW (50-100 nm diameter) suspension onto the glass. Consequently, this nanowire mesh was laminated over PEDOT: PSS thin films. Pressure was applied for efficient transfer of nanowires. In order to further investigate the process, different PEDOT: PSS thicknesses (25, 50, 75, 100 and 125 nm) were evaluated. It was observed that with increasing PEDOT: PSS thickness, roughness were decreased with increase in conductivity. As a result, flat, conductive and partially transparent surface was obtained with Ag NWs laminated over PEDOT: PSS with a thickness of 125 nm. Bulk heterojunction solar cells were than fabricated both with ITO thin films and Ag NW networks. Comparable power conversion efficiencies (about 4.2 %) to that of devices fabricated on ITO thin films with Ag NW networks. Moreover, Yu et. al. reported a Ag NW/polymethacrylate composite electrode and used this as a bottom electrode in OSCs [56]. The composite electrode consisted of a stack of two types of Ag NWs. One was synthesized in-house by the researchers and the other one was purchased from Blue Nano Inc. The diameter and length of the synthesized nanowires were 60 nm and 4-10 μm, respectively. On the other hand, the diameter and the length of purchased nanowires were 90 nm and 30-50 μm, respectively. Short Ag NWs were selected for large surface coverage and the long ones were utilized to improve conductivity. Bifunctional methacrylate monomer is coated over the stack of long Ag NWs and cured. Then, the resulting polymethacrylate composite electrode was peeled off from the glass surface and placed over short Ag NW network over glass. By this process, roughness problem was eliminated. A power conversion efficiency of 3.28% was obtained from this solar cell, having PEDOT: PSS as the hole transport layer, P3HT:PCBM as the active layer and LiF as the electron transport layer. This efficiency value was found comparable to that of a control device fabricated on ITO bottom electrode (3.34 %).

On the other hand, Krantz et al. compared the efficiencies of devices fabricated using thermally evaporated silver and Ag NW top electrodes [57]. The device structure of the inverted OSCs was ITO / aluminum doped zinc oxide (AZO)/P3HT: PCBM/PEDOT: PSS. Reference device was fabricated by evaporating 100 nm of Ag

and the power conversion efficiency was calculated as 3 %. Ag NW electrode layers were spray deposited over the device. Electrodes had a sheet resistance of 7 ohm/square and an average transmittance of over 85 % within a wavelength range of 400-800 nm. When the device characteristics were investigated, comparable power conversion efficiency values were obtained to that of the reference device fabricated by thermal evaporation of Ag as the top electrode. Lee et al. also used Ag NWs as top electrodes for organic photovoltaics [58]. They choose a different method for coating. They cleaned glass substrates in an aqueous poly-L-lysine solution for 5 minutes. Then nanowire suspension was drop casted. The reason for using poly-L-lysine is to prevent aggregation of nanowires. Dried nanowires were heated up to 180 °C for the fusion of nanowires. At the end of the process, Ag NW networks had a sheet resistance of 15-25 ohm/square and an optical transmittance of 75-85 %. However, the roughness of the nanowires was found to be too high (200-300 nm). To lower the roughness, approximately 2×10^4 psi pressure was applied by a hydraulic press for 30 seconds. Then these electrodes were used as the top contacts in a device having an architecture of, ITO/ 25 nm copper phthalocyanine(CuPc) / 50 nm C_{60} /10 nm bathocuproine (BCP). For comparison, one more device with a vacuum deposited Ag cathode was also fabricated. The obtained efficiencies of devices with and without nanowires were 0.63 and 1.1 %, respectively.

3. 3. EXPERIMENTAL DETAILS

3. 3. 1. Organic Solar Cell Devices using Ag NW Network as Bottom Electrode

3. 3. 1. 1. Fabrication of Ag NW Network as Bottom Electrode

Ag NWs were synthesized according to the polyol method as mentioned before and purified using the same purification procedure as stated in Part 2. 3. 1. Then, glass substrates were cut into 2.54 cm x 2.45 cm rectangles. Substrates were cleaned thoroughly by sonication in acetone (99.8%), isopropyl alcohol (99.8%) and finally deionized water (18.3 MΩ) for 15 minutes each. Oxygen plasma was used for further cleaning in order to make sure that no organic residues remained. Substrates were placed over a hot plate at 100°C for the instant removal of ethanol. A simple spray

mask was prepared using kapton tape to deposit nanowires only onto an area of 2.54 cm x 1.2 cm. Then, Ag NW-ethanol solution was deposited over the glass substrates using a simple N_2 fed air brush. All spray coatings were carried out at a pressure of 2 atm and sprayed 10 cm away from the hot plate. Coating was carried out until a sheet resistance of 40-50 ohm/ square was obtained. In order to lower the roughness of the Ag NW networks, a heat treatment was carried out by following the route stated by Coskun et al [59]. A pre-cleaned glass was placed over the networks and a weight of 200 gr was placed over it. Samples were kept at 200°C for 20 minutes. By this process, residual PVP covering the surface of nanowires was eliminated and the roughness at contact points of Ag NWs were lowered [59].

3. 3. 1. 2. Fabrication of Solar Cells

OSC devices using Ag NW networks and poly(3,4-ethylenedioxythiophene) polystyrene sulfonate (PEDOT: PSS) Clevious 4083 as bottom electrodes was used for this architecture. First, PEDOT: PSS was filtered with polyvinylidene difluoride (PVDF) filters with a pore size of 0.45 μm. Then, PEDOT:PSS /isopropyl alcohol with a volume ratio of (4:1) was spin coated at 1000 rpm for 45 seconds over as deposited and annealed Ag NW networks. Samples were annealed for 20 minutes at 110°C. For the active layer, poly(3-hexylthiophene) (P3HT) was used as donor layer and phenyl-C60-butyric acid methyl ester $PC_{60}BM$ was used as acceptor layer. P3HT:$PC_{60}BM$ (1:0.8) solution at a solution concentration of 2 % was dissolved in dichlorobenzene and mixed for 8 hours at 70 $^{\circ}$C in a glovebox. Solution was filtered through PTFE filters with a pore size of 0.22 μm and spin coated at 750 rpm for 45 seconds. Lastly as the electron transport and collection layer, 0.6 nm LiF and 100 nm Al was evaporated via physical vapor deposition (PVD) using a shadow mask, respectively.

In order to compare the device characteristics, a similar device was prepared on commercially available ITO (sheer resistance 4-10 ohm/sq and transmittance above 82%) anode. Similar to the previous architecture, bottom contact was set at an area of 2.54 cm x 1.2 cm. Therefore, this area was covered with a tape to prevent etching. ITO coated glasses were kept in a solution containing 49 vol. % hydrochloric (HCl) and 1 vol. % nitric acid (HNO_3) solutions for 4 minutes at 65 $^{\circ}$C to etch the desired pattern. Afterwards, substrates were cleaned by sonication with toluene, isopropyl alcohol

(99.8%) and finally deionized water (18.3 MΩ) for 15 minutes each. Then, oxygen plasma was used to clean the ITO surface from organic residuals. Other layers were spin coated and evaporated similarly onto ITO. For the contact points, part of the polymer layer over the ITO was wiped off with chloroform. Device characteristics were measured through the contact points on ITO surface and on LiF/Al thin films.

To sum up, two solar cells were fabricated. In the first device architecture Ag NW network was used as the anode layer, while PEDOT: PSS was used as the hole transport layer, P3HT:PC$_{60}$BM was used as active layer, 0.6nm LiF was used as electron transport layer and 100 nm Al was used as the cathode layer. Whereas in the second device architecture, ITO was used as the anode layer, while all other layers remained the same.

3. 3. 2. Inverted OSC Devices Using Ag NW Networks as Top Electrode

3. 3. 2. 1. Fabrication of Ag NW Network Top Electrodes

Synthesized and purified Ag NWs within ethanol solution was spray coated over pre-cleaned glass substrates. Before coating process, glasses were masked by a kapton tape. Three electrodes were prepared each having an approximate area of 0.3 cm x 2 cm. Coating process was continued until the resistance of the stripes was measured between 20 and 30 ohm. Then, these substrates were spin coated by a polydimethylsiloxane (PDMS) layer (Sylgard 184). For the preparation of PDMS, silicon elastomer and its curing agent was mixed at a ratio of 10:1 and the mixture was placed in a vacuum furnace for half an hour to eliminate the bubbles inside the mixture. This solution was spin coated onto Ag NW networks at 500 rpm for 40 seconds. For curing, samples were kept in a furnace at 160°C for 30 minutes. Cured PDMS layer was lifted from the glass surface by the help of tweezer in hot water 50°C.This process allowed the transfer of Ag NW network from glass to PDMS surface.

3. 3. 2. 2. Fabrication of Inverted Solar Cell

In inverted OSC architecture, Ag NW network was used as the top electrode. Therefore, firstly indium tin oxide (ITO) coated glass substrates were etched using

acidic solutions as described before. Similar to previous architecture, bottom contact was patterned at an area of 2.54 cm x 1.2 cm. Therefore, this area was covered with a tape to prevent etching. Afterwards, zinc oxide (ZnO) was deposited onto ITO as the electron transport layer. All chemicals used for ZnO layer were purchased from Sigma Aldrich and used without further purification. One day before the fabrication, ZnO solution was prepared by mixing 0.4 gram of zinc acetate dehydrate ($\geq$ 99.0 %) and 0.10 ml of ethanolamine ($\geq$ 98.0 %) in 5 ml of 2-methoxyethanol (anhydrous, 99.8 %) solution at room temperature. This solution was spin coated over ITO at 4000 rpm for 60 seconds and annealed at 150°C for 20 minutes. For the deposition of the active layer, P3HT:PC$_{71}$BM solution was prepared. Poly(3-hexylthiophene) (P3HT) was used as donor and phenyl-C71-butyric acid methyl ester PC$_{71}$BM was used as the acceptor layer. P3HT:PC$_{71}$BM (1:0.8) solution at a concentration of 2 % was dissolved in dichlorobenzene and the solution was mixed for 8 hours at 70 ^{o}C in a glovebox. After filtering the solution using the PTFE filters with a pore size of 0.22μm, the solution was spin coated onto ITO/ZnO substrates at 750 rpm for 45 seconds. Consequently, PEDOT: PSS (Ossila HTL) layer was spin coated onto organic active layer at 2500 rpm for 60 seconds to act as the hole transport layer. Lifted PDMS, with Ag NWs as described before, was slightly shifted and placed over the fabricated ITO/ZnO/ P3HT:PC$_{71}$BM /PEDOT: PSS device structure. As the PDMS was not cured fully, it adhered well to the devices. Devices were heated at 70°C for 20 minutes under vacuum to eliminate the bubbles at the contact surface. Then, the shifted part of the Ag NW/PDMS was turned upside down and point contacts were prepared over Ag NW network stripes using Ag paste. Alternatively, 100 nm of gold (Au) was evaporated using PVD method to fabricate the reference samples for comparison.

To sum up, two solar cells were fabricated. In the first device architecture Ag NW network was used as anode, PEDOT: PSS was used as the hole transport layer, P3HT:PC$_{71}$BM was used as the active layer, 0.6 nm LiF was used as the electron transport layer and 100 nm Al was used as cathode. In the second device architecture, on the other hand, ITO was used as the anode and other layers were remained the same.

3. 4. CHARACTERIZATION METHODS

3. 4. 1. Scanning Electron Microscopy (SEM)

Synthesized Ag NWs were analyzed using a field emission scanning electron microscope (FE-SEM) (Nova NanoSEM 430) operated at 10 and 20 kV. In order to analyze nanowires in solution, SEM samples were prepared by drop casting Ag NW solution over pre-heated silicon wafers, which were then placed onto SEM stubs by carbon tape.

3. 4. 2. Atomic Force Microscopy (AFM)

A Veeco MultiMode V was used to investigate the topography of the Ag NW /PDMS samples in tapping mode.

3. 4. 3. Transmittance Measurements (UV-VIS)

An Agilent 8453 UV-VIS spectrophotometer was used to measure the direct transmittance of the Ag NW/glass samples within the visible range (400-700 nm).

3. 4. 4. Photovoltaic Characteristics

Device measurements were carried under AM 1.5 solar simulator having 100 mW / cm^2 of power. Data was collected using the Lab tracer program.

3. 5. RESULTS

3. 5. 1. Ag NW Network and ITO as Bottom Electrode and Device Fabrication

Bottom electrode was fabricated according to a route stated in the previous section. In order to measure the optical transmittance of the nanowire networks, UV-VIS was used. Optical transmittance of spray coated Ag NW networks having sheet resistance of 40 Ω/ square is 80 % at a wavelength of 550 nm as shown in Figure 3.7.
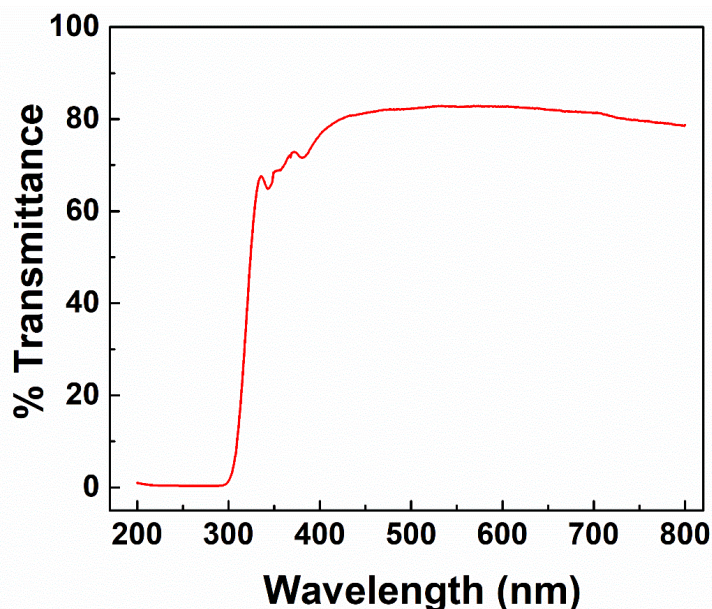
Figure 3. 7 Optical transmittance spectrum of sprayed coated Ag NW network on glass.

In this architecture, major challenge faced during the fabrication was the surface roughness of Ag NW networks. Ag NW networks (as coated) were rougher compared to ITO (RMS roughness 24.8 nm [60]). This problem was overcome by the press annealing as stated by Coskun et al. [59]. After the spray coating process, samples were press annealed. The roughest part of the network was where the NWs overlap. Therefore, during press annealing, these points were targeted. SEM images provided in Figure 3.8 showed the decreased roughness at the nanowire junctions. Thickness of the polymer layer (residual PVP layer) surrounding the nanowires found to decrease and thus, the sheet resistance of the network was found to decrease.

70
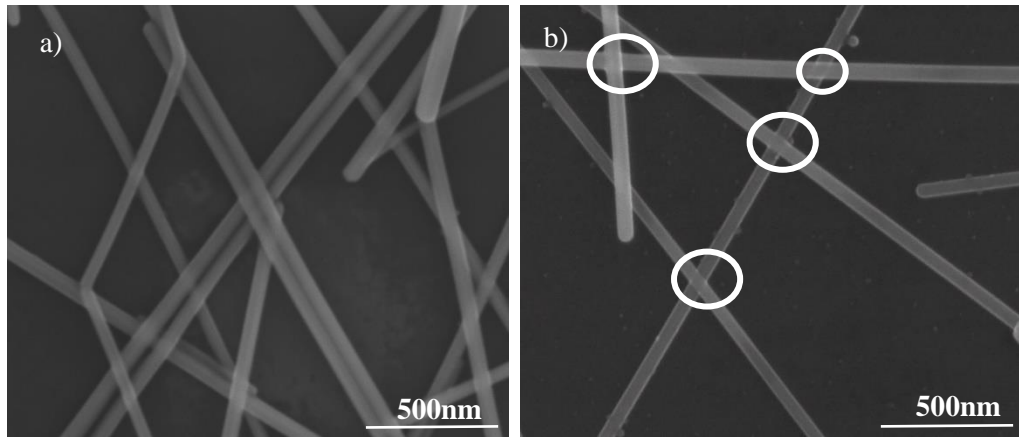
Figure 3. 8 SEM images of Ag NW networks (a) before and (b) after press annealing.

Solar cells were fabricated according to the route stated in the previous section. Schematic device architecture and photographs are provided in Figures 3.9 and 3.10 respectively. PEDOT: PSS and P3HT: $PC_{60}BM$ solutions were spin coated and LiF and Al layers were evaporated through a shadow mask via PVD.
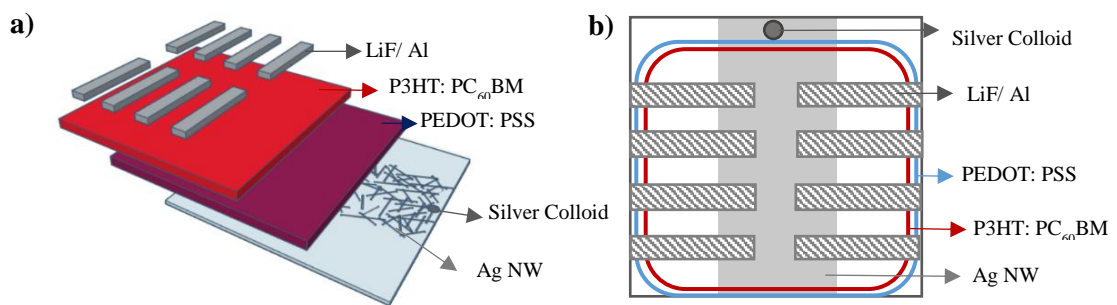
Figure 3. 9 Schematic architecture of Ag NW network bottom electrode devices (a) side view and (b) top view.
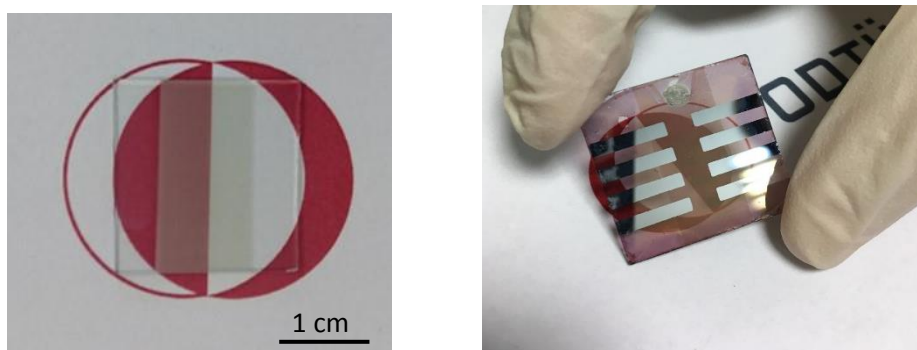
Figure 3. 10 Photographs of Ag NW network contact (bottom electrode) on glass (left) and finalized device (right).

As mentioned before, control devices with ITO anodes were also fabricated. The main advantage of ITO thin films was their lower roughness values compared to the Ag NW network. Therefore, the number of devices that worked properly without short circuiting was higher on ITO. However, figure of merit optical transparency and conductivity of both the ITO thin films and Ag NW networks were comparable. The current density and voltage characteristics of the fabricated devices were provided in Figure 3.11. Calculated photovoltaic parameters are given in Table 3.1.
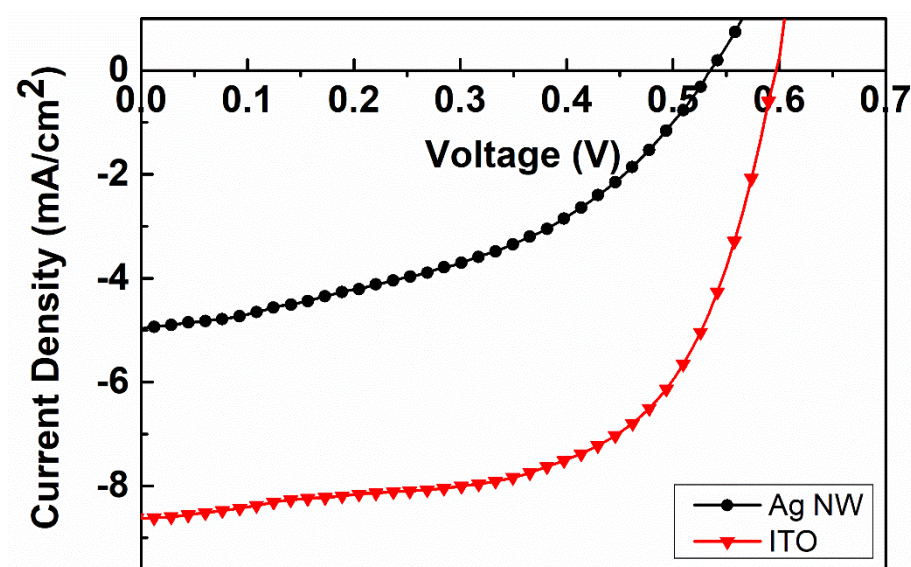
Figure 3. 11 Current density (J) and voltage (V) characteristics of fabricated bottom electrode devices.

The device with ITO thin film had higher fill factor compared to one with Ag NWs. Ag NWs had slightly lower V_{OC} value compared to the devices fabricated using ITO thin film. This behavior was attributed to the higher roughness value of the Ag NW network.

Table 3. 1 Calculated photovoltaic parameters of devices with Ag NW network and ITO thin film anodes as bottom electrode.

Anode Material	V_{oc} (V)	J_{sc} (mA/cm^2)	FF (%)	PCE (%)
Ag NW network	0.53	4.99	43	1.13
ITO thin film	0.6	8.56	66.4	3.15

3. 5. 2. Ag NW Network and Au Thin Film as Top Electrode and Device Fabrication

Top electrodes having Ag NW network and PDMS structure was prepared according to the route stated in previous section. Some of the Ag NWs were found as embedded in the PDMS layer, which resulted in a highly flexible layer. Photos of the Ag NW/PDMS electrodes fabricated in this work is provided in Figure 3. 12.
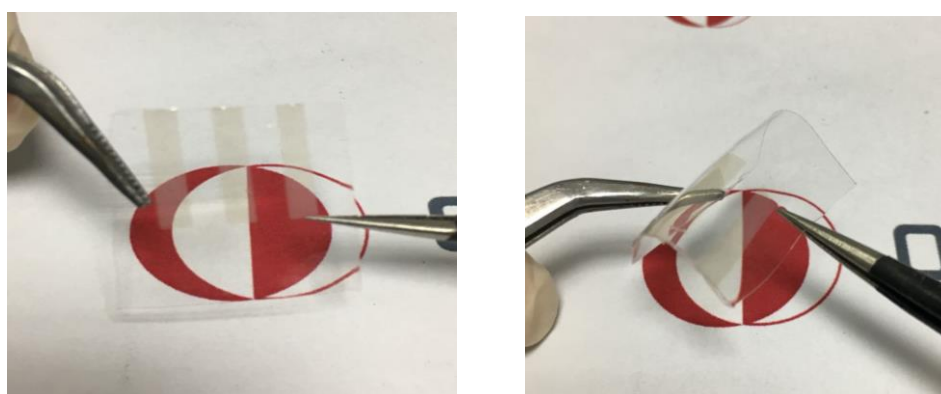
Figure 3. 12 Photographs showing flexibility and transparency of the fabricated Ag NW/PDMS top electrodes.

Roughness was the main problem for the Ag NW networks and especially if they are used as bottom electrodes. To eliminate this problem, device architecture was changed to inverted OSCs. These top electrodes were investigated further using SEM and AFM. Top view and cross-sectional SEM images of Ag NW/PDMS top electrodes are provided in Figure 3.15 (a) and (b), respectively. From Figure 3.13 (a), some Ag NWs seemed as if they were sticking out from the PDMS layer. However, the cross-sectional

SEM image (Figure 3. 13 (b)) showed that, there were no Ag NWs over the surface of PDMS.
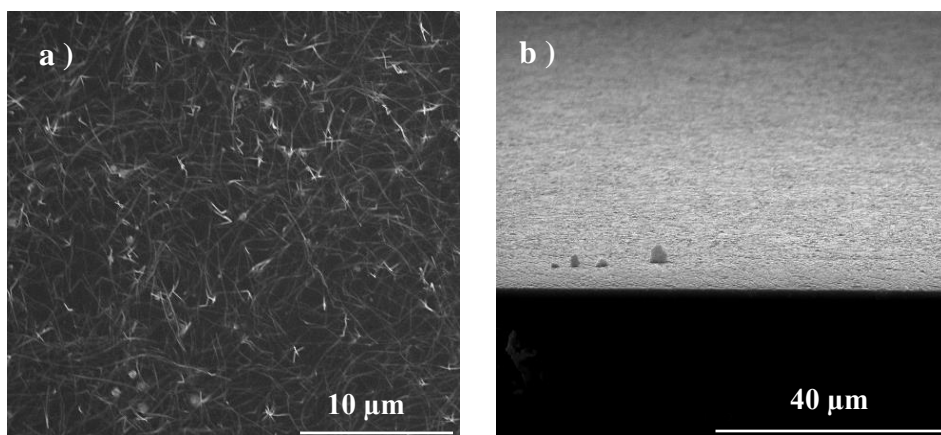
Figure 3. 13 (a) Top view (b) cross-sectional SEM images of top electrodes.

For further investigation, surface roughness of the Ag NW/PDMS electrodes was investigated by AFM (Figure 3.14 and Figure 3.15). AFM images of bare PDMS and Ag NW/PDMS composites are provided in Figure 3.14 and 3.15, respectively. Bare PDMS surface was not smooth and a few cracks were observed similar on the surface. Afterwards, PDMS/Ag NW surfaces were characterized. Similar cracks were present on the Ag NW/PDMS composite surface. Average and maximum roughness values of both images were calculated and presented in Table 3.2. Roughness of Ag NW/PDMS composites was found to be larger than the bare PDMS sample.
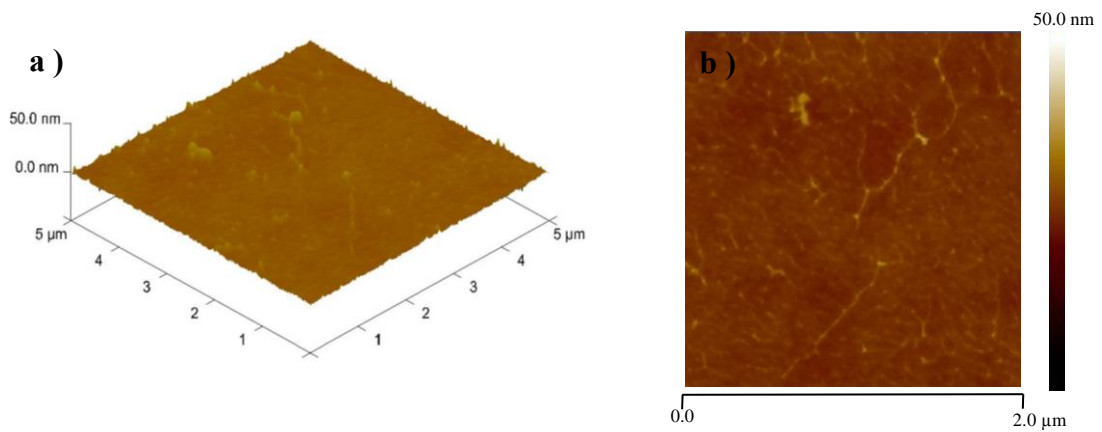
Figure 3. 14 AFM images of bare-PDMS in (a) 3D and (b) 2D.
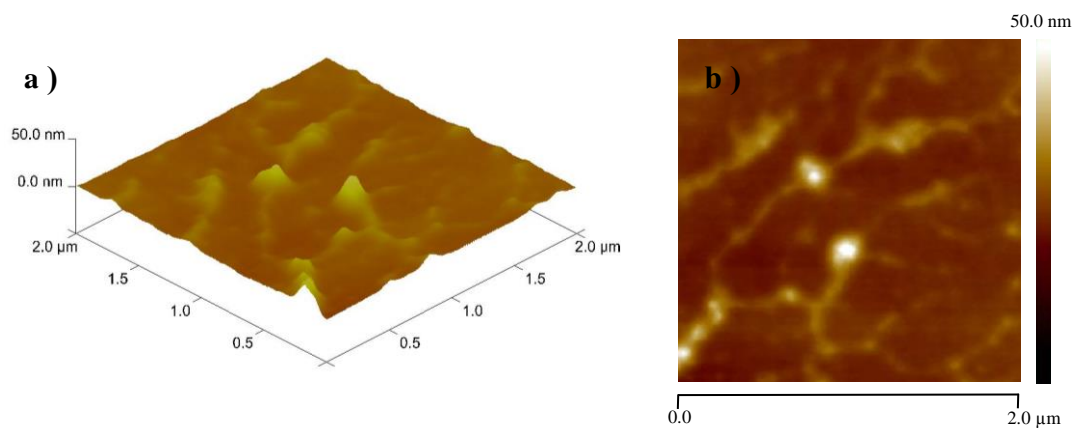
Figure 3. 15 AFM images of Ag NW-PDMS in (a) 3D and (b) 2D.

Table 3. 2 Roughness values obtained from AFM measurements.

Sample	Average Roughness (nm)	Maximum Roughness (nm)
Bare PDMS	0.710	13.4
Ag NW/PDMS	1.90	32.7

Solar cells were fabricated according to the fabrication route described in the previous section. Device architecture is schematically shown in Figure 3.16.
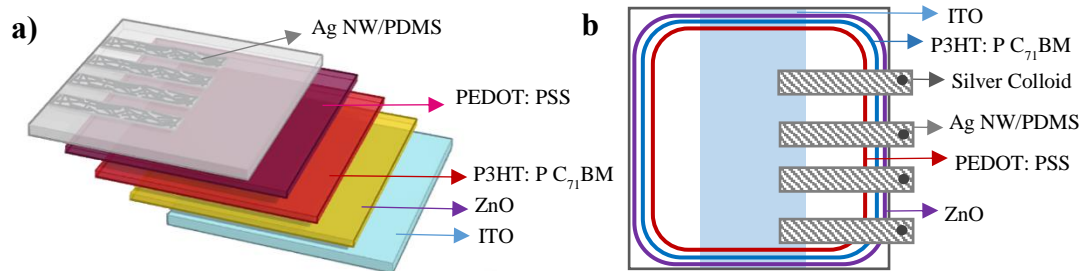
Figure 3. 16 Schematic device architecture of top electrode devices in (a) side-view and in (b) top-view

Figure 3. 17 Photographs of an inverted solar cell with Ag NW/PDMS top electrode (left) and Au top electrode (right).

The current density and voltage characteristics of the fabricated devices can be observed in Figure 3.18 and calculated photovoltaic parameters are provided in Table 3.3. When the J-V characteristics of the fabricated devices are compared, it is observed that FF of the both devices are the same and V_{OC} values are really close to each other.
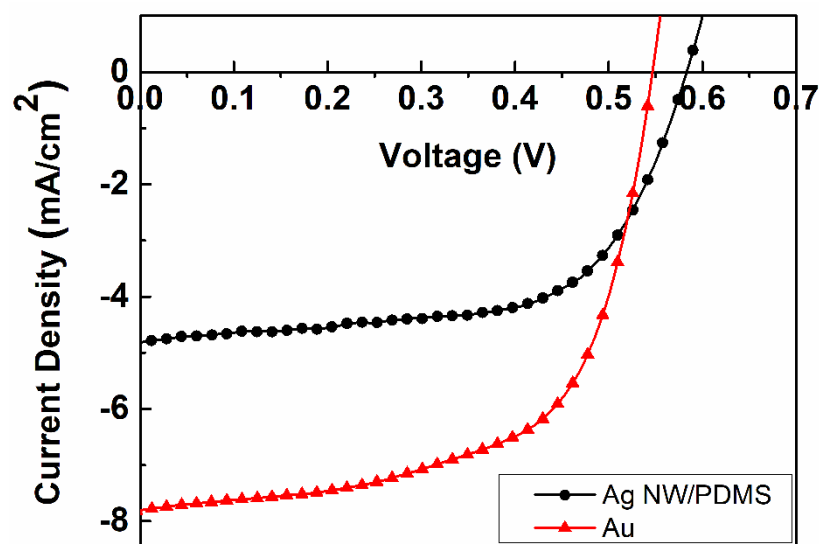
Figure 3. 18 Current density (J) and voltage (V) characteristics of fabricated top electrode solar cells.

Table 3. 3 Calculated photovoltaic parameters of devices with Ag NW/PDMS and Au top electrodes.

Anode Material	V_{oc} (V)	J_{sc} (mA/cm^2)	FF (%)	PCE (%)
Ag NW /PDMS	0.58	4.81	62	1.73
Au (100 nm)	0.54	7.84	62	2.62

Similar shunt resistances (inverse slope at I_{SC}) were obtained from the fabricated devices, while the series resistance (inverse slope at V_{OC}) for Ag NW/PDMS top contacted device was a little higher. This might be due to improper mating between PDMS and PEDOT:PSS due to residual air bubbles.

CHAPTER 4

CONCLUSIONS AND FUTURE RECOMMENDATIONS

4. 1. CONCLUSIONS

In the second chapter of the thesis, EM shielding behavior of the Ag NWs were investigated. Main aim was to use Ag NWs to impart conductivity to various samples and to analyze their EM interaction characteristics at a frequency range of 18 - 40 GHz. EM characteristics of Ag NW modified materials were measured by the free space method. Different substrates were selected in order to demonstrate electromagnetic shielding behavior of Ag NWs. PET was selected for transparent and flexible applications. Highest SE was obtained from the Ag NW networks on PET with a sheet resistance of 1kohm/square. This sample absorbed 40 % and reflected 10% of the incident wave. However, it transmitted half of the incident wave, which was really high. In order to lower this value, Ni thin films were deposited onto Ag NW networks on PET substrates. The transmission and reflection percentages were found to highly depend on the evaporated Ni thin film thickness. Even evaporation of a 5 nm thin layer Ni over Ag NW network (with a sheet resistance of 1 kohm) improved its reflection to 30 % and absorption to 45 %. Transmission values were found to decrease significantly. Filter paper, textile and felt were also used as substrates in this work with an intention to make use of their 3D porous nature. For these substrates, inner reflections were increased and transmission values were decreased due to their microstructure and 3D deposition of Ag NWs. Substrate change enhanced the shielding behavior by increasing the absorption by approximately 5% and reflection by 10 %. Among the textile samples, the one with a resistance of 100 ohm showed the best absorption dominant shielding performance. Percent absorption values were increased up to 66 %. Only 5 % of the incident wave was transmitted inside. Among

felt samples, sample with a resistance of 100 ohm showed reflection dominant shielding and transmitted only 3 % of the incident wave. Approximately 40 % of the wave was absorbed and the remaining portion was reflected.

In the third chapter, Ag NW networks were used as bottom and top electrodes for OSCs. Motivation was to replace commercially available ITO thin films or evaporated metals with solution deposited Ag NW networks. Firstly, Ag NWs were used to replace ITO in a device structure of ITO / PEDOT: PSS / P3HT: $PC_{60}BM$ / LiF / Al. Control device fabricated with ITO anode showed a power conversion efficiency of 3.15 %, while the device with spray coated transparent Ag NW network had a power conversion efficiency of 1.13 %. This much difference between the obtained power conversion efficiencies was due to the high roughness of Ag NW networks. Although, press annealing was applied following the deposition of Ag NW networks, it was really hard to prevent short-circuits in this structure. Secondly, Ag NW networks was used as top contacts in OSCs in order to replace evaporated Au thin films with transparent Ag NW/PDMS in a device structure of ITO/ ZnO/ P3HT:$PC_{71}BM$/ PEDOT: PSS /Au. This use of Ag NW networks in this structure enabled the fabrication of semi-transparent OSCs, which was not possible to fabricate using conventional thin film evaporation method for the contact formation. Control devices with Au top electrodes had a power conversion efficiency of 2.62 %, while the device with Ag NW/PDMS had a power conversion efficiency of 1.73 %. Main problem for this structure was the physical placement of PDMS over the PEDOT: PSS layer without leaving air bubbles. This was also responsible with the resulting low efficiency of fabricated devices.

4. 2. FUTURE RECOMMENDATIONS

Frequencies larger than 27 - 30 GHz are problematic due to water absorption and decreased wavelength of the electromagnetic wave. Calibration prior to each measurement and normalization were not enough to overcome scattering. Measurements had some errors due to the setup calibration.

Ag NW networks are promising nanomaterials and alternatives to commercially available ITO thin films. Even though better optoelectronic properties (sheet

resistance, optical transmittance) was obtained from Ag NWs compared to ITO thin film, OSC efficiencies when Ag NWs were used as contacts were lower compared to the devices fabricated with ITO. Using Ag NW networks as bottom contact was rather difficult compared to using these networks as top contacts in OSCs. Roughness was the biggest problem, which should be overcome in order to prevent device from short-circuits. Upon the use of Ag NW networks as the top contacts, the biggest problem was placing the PDMS substrate with Ag NWs onto PEDOT:PSS film without leaving air bubbles. Different placement strategies and post placement strategies are worthwhile to investigate.

REFERENCES

[1]   J. Essam, H. Search, C. Journals, A. Contact, and M. Iopscience, "Percolation theory," *Reports Prog. Phys.*, vol. 43, p. 833, 1980.

[2]   S. I. White *et al.*, "Electrical percolation behavior in silver nanowire-polystyrene composites: Simulation and experiment," *Adv. Funct. Mater.*, vol. 20, no. 16, pp. 2709–2716, 2010.

[3]   S. Coskun, E. Selen Ates, and H. Emrah Unalan, "Optimization of silver nanowire networks for polymer light emitting diode electrodes," *Nanotechnology*, vol. 24, no. 12, 2013.

[4]   O. Ergun, S. Coskun, Y. Yusufoglu, and H. E. Unalan, "High-performance, bare silver nanowire network transparent heaters," *Nanotechnology*, vol. 27, no. 44, 2016.

[5]   A. R. Madaria, A. Kumar, and C. Zhou, "Large scale, highly conductive and patterned transparent films of silver nanowires on arbitrary substrates and their application in touch screens," *Nanotechnology*, vol. 22, no. 24, 2011.

[6]   M. Amjadi, A. Pichitpajongkit, S. Lee, S. Ryu, and I. Park, "Highly stretchable and sensitive strain sensor based on silver nanowire-elastomer nanocomposite," *ACS Nano*, vol. 8, no. 5, pp. 5154–5163, 2014.

[7]   Y. Nie, H. H. He, and L. You, "Thin electromagnetic wave absorber containing Fe-Co alloy for quasi-microwave band," *INTERMAG Asia 2005. Dig. IEEE Int. Magn. Conf. 2005.*, vol. 33, no. 6, pp. 4459–4464, 2005.

[8]   "Microwave characterization and modelization of magnetic granular materials," *Journal of Applied Physics*, Vol 73, No 10." .

[9]   "Preparation and microwave characterization of spherical and monodisperse Co20Ni80 particles," J*ournal of Applied Physics*, Vol 76, No 10." .

[10]   D. D. Chung, "Electromagnetic interference shielding effectiveness of carbon materials," *Carbon N. Y.*, vol. 39, no. 2, pp. 279–285, 2001.

[11]   P. Liu and Y. Huang, "Synthesis of reduced graphene oxide-conducting polymers-Co3O4 composites and their excellent microwave absorption properties," *RSC Adv.*, vol. 3, no. 41, p. 19033, 2013.

[12]   J. Jiang *et al.*, "Microwave absorption properties of core double-shell FeCo/C/BaTiO $_3$ nanocomposites," *Nanoscale*, vol. 6, no. 8, pp. 3967–3971, 2014.

[13] Z. Wang, L. Wu, J. Zhou, B. Shen, and Z. Jiang, "Enhanced microwave absorption of Fe3O4 nanocrystals after heterogeneously growing with ZnO nanoshell," *RSC Adv.*, vol. 3, no. 10, p. 3309, 2013.

[14] C. He *et al.*, "Facile synthesis of hollow porous cobalt spheres and their enhanced electromagnetic properties," *J. Mater. Chem.*, vol. 22, no. 41, p. 22160, 2012.

[15] R. Kumar *et al.*, "Improved microwave absorption in lightweight resin-based carbon foam by decorating with magnetic and dielectric nanoparticles," *RSC Adv.*, vol. 4, no. 45, p. 23476, 2014.

[16] D. P. Sun, Q. Zou, Y. P. Wang, Y. J. Wang, W. Jiang, and F. S. Li, "Controllable synthesis of porous Fe3O4@ZnO sphere decorated graphene for extraordinary electromagnetic wave absorption.," *Nanoscale*, vol. 6, no. 12, pp. 6557–6562, 2014.

[17] J. Kónya and N. M. Nagy, "5 - Interaction of Radiation with Matter," *Nucl. Radiochem.*, pp. 83–127, 2012.

[18] P. A. Tipler and G. Mosca, *Physics for Scientists and Engineers*. 2009.

[19] E. Sciences, S. Imagery, A. Photos, S. Imagery, E. Resources, and R. Basics, "Radar Basics," no. C. pp. 1–5, 2016.

[20] S. F. Bands, "Satellite frequency bands / Telecommunications & Integrated Applications." pp. 4–5, 2016.

[21] W. Callister and D. Rethwisch, *Materials science and engineering: an introduction*, vol. 94. 2007.

[22] J. Huo, L. Wang, and H. Yu, "Polymeric nanocomposites for electromagnetic wave absorption," *J. Mater. Sci.*, vol. 44, no. 15, pp. 3917–3927, 2009.

[23] J. W. Gooch and J. K. Daher, *Electromagnetic shielding and corrosion protection for aerospace vehicle*. 2007.

[24] F. Wu, Z. Xu, Y. Wang, and M. Wang, "Electromagnetic interference shielding properties of solid-state polymerization conducting polymer," *R. Soc. Chem. Adv.*, vol. 4, pp. 38797–38803, 2014.

[25] Anritsu Company, "Lightning 37xxxE Vector Network Analyzer Operation Manual," no. July, 2008.

[26] F. Shahzad *et al.*, "Electromagnetic interference shielding with 2D transition metal carbides (MXenes)," *Science*, vol. 353, no. 6304, pp. 1137–1140, 2016.

[27] W. Zhao, M. Li, Z. Zhang, and H. X. Peng, "EMI shielding effectiveness of silver nanoparticle-decorated multi-walled carbon nanotube sheets," *Int. J. Smart Nano Mater.*, vol. 1, no. 4, pp. 249–260, 2010.

[28] Y. H. Yu *et al.*, "Electrical, morphological, and electromagnetic interference shielding properties of silver nanowires and nanoparticles conductive composites," *Mater. Chem. Phys.*, vol. 136, no. 2–3, pp. 334–340, 2012.

[29] J. Ma, M. Zhan, and K. Wang, "Ultralightweight silver nanowires hybrid polyimide composite foams for high-performance electromagnetic interference shielding," *ACS Appl. Mater. Interfaces*, vol. 7, no. 1, pp. 563–576, 2015.

[30] F. Fang, Y.-Q. Li, H.-M. Xiao, N. Hu, and S.-Y. Fu, "Layer-structured silver nanowire/polyaniline composite film as a high performance X-band EMI shielding material," *J. Mater. Chem. C*, vol. 4, pp. 4193–4203, 2016.

[31] C. Morari and I. Bălan, "Methods for determining shielding effectiveness of materials," *Electroteh. Electron. Autom.*, vol. 63, no. 2, pp. 126–136, 2015.

[32] P. Policy, "RF network analyzer basics tutorial," *Spectrum*. pp. 1–4, 2010.

[33] Agilent Technologies, "Advanced Calibration Techniques for Vector Network Analyzers," *Mil. Commun. Radars*, pp. 1–86, 2006.

[34] S. Coskun, B. Aksoy, and H. Emrah Unalan. "Polyol Synthesis of Silver Nanowires: An Extensive Parametric Study," *Cryst, Growth Des.*, 11, 2015, 4963-4969

[35] V. Devabhaktuni, M. Alam, S. Shekara Sreenadh Reddy Depuru, R. C. Green, D. Nims, and C. Near, "Solar energy: Trends and enabling technologies," *Renew. Sustain. Energy Rev.*, vol. 19, pp. 555–564, 2013.

[36] Retrieved from http://www.environment.gov.au/climate-change/climate-science-data/climate-science/greenhouse-effect.

[37] A. V. Herzog, T. E. Lipman, and D. M. Kammen, "Renewable energy sources," *Encycl. Life*, pp. 1–63, 2001.

[38] A. M. Bagher, "Introduction to Organic Solar Cells," *Sustain. Energy*, vol. 2, no. 3, pp. 85–90, 2014.

[39] R. W. Miles, K. M. Hynes, and I. Forbes, "Photovoltaic solar cells : An overview of state-of-the-art cell development and environmental issues," vol. 51, 2005.

[40] H. Hoppe and N. S. Sariciftci, "Organic solar cells: An overview," *J. Mater. Res.*, vol. 19, no. 7, pp. 1924–1945, 2004.

[41] V. I. Madogni, B. Kounouhéwa, A. Akpo, M. Agbomahéna, S. A. Hounkpatin, and C. N. Awanou, "Comparison of degradation mechanisms in organic photovoltaic devices upon exposure to a temperate and a subequatorial climate," *Chem. Phys. Lett.*, vol. 640, pp. 201–214, 2015.

[42] M. Wang and I. G. Hill, "Fluorinated alkyl phosphonic acid SAMs replace PEDOT:PSS in polymer semiconductor devices," *Org. Electron. physics, Mater. Appl.*, vol. 13, no. 3, pp. 498–505, 2012.

[43] S. Holliday, Y. Li, and C. K. Luscombe, "Recent advances in high performance donor-acceptor polymers for organic photovoltaics," *Prog. Polym. Sci.*, vol. 70, pp. 34–51, 2017.

[44] J. Rn Rostalski and D. Meissner, "Monochromatic versus solar e$ciencies of organic solar cells," *Sol. Energy Mater. Sol. Cells*, vol. 61, pp. 87–95, 2000.

[45] T. B. Singh and N. S. Sariciftci, "Progress in Plastic Electronics Devices," *Annu. Rev. Mater. Res.*, vol. 36, no. 1, pp. 199–230, 2006.

[46] Myers, D. R.; Kurtz, S. R.; Whitaker, C.; Townsend, T. (2000). Preliminary Investigations of Outdoor Meteorological Broadband and Spectral Conditions for Evaluating Photovoltaic Modules and Systems. Program and Proceedings: NCPV Program Review Meeting 2000, 16-19 April 2000, Denver, Colorado.

[47] J. Rostalski and D. Meissner, "Photocurrent spectroscopy for the investigation of charge carrier generation and transport mechanisms in organic p/n-junction solar cells," *Sol. Energy Mater. Sol. Cells*, vol. 63, pp. 37–47, 2000.

[48] S. Günes, H. Neugebauer, and N. S. Sariciftci, "Conjugated polymer-based organic solar cells," *Chem. Rev.*, vol. 107, no. 4, pp. 1324–1338, 2007.

[49] I. Riedel and V. Dyakonov, "Influence of electronic transport properties of polymer-fullerene blends on the performance of bulk heterojunction photovoltaic devices," *Phys. Status Solidi Appl. Res.*, vol. 201, no. 6, pp. 1332–1341, 2004.

[50] R. Timmreck, S. Olthof, K. Leo, and M. K. Riede, "Highly doped layers as efficient electron-hole recombination contacts for tandem organic solar cells," *J. Appl. Phys.*, vol. 108, no. 3, 2010.

[51] D.-S. Leem, A. Edwards, M. Faist, J. Nelson, D. D. C. Bradley, and J. C. de Mello, "Efficient Organic Solar Cells with Solution-Processed Silver Nanowire Electrodes," *Adv. Mater.*, vol. 23, no. 38, pp. 4371–4375, 2011.

[52] F. Guo *et al.*, "ITO-free and fully solution-processed semitransparent organic solar cells with high fill factors," *Adv. Energy Mater.*, vol. 3, no. 8, pp. 1062–1067, 2013.

[53] L. Hu, H. S. Kim, J. Lee, P. Peumans, and Y. Cui, "Scalable Coating and Properties of transparent Ag nanowire," *ACS Nano*, vol. 4, no. 5, pp. 2955–2963, 2010.

[54] L. Yang, T. Zhang, H. Zhou, S. C. Price, B. J. Wiley, and W. You, "Solution-Processed Flexible Polymer Solar Cells with Silver Nanowire Electrodes," *ACS Appl. Mater. Interfaces*, vol. 3, no. 10, pp. 4075–4084, 2011.

[55] Gaynor W, Burkhard G F, McGehee M D and Peumans P. (2011). " Smooth Nanowire/Polymer Composite Transparent Electrodes," *Adv. Mater.* 23 2905–10

[56] Z. Yu, L. Li, Q. Zhang, W. Hu, and Q. Pei, "Silver nanowire-polymer composite electrodes for efficient polymer solar cells," *Adv. Mater.*, vol. 23, no. 38, pp. 4453–4457, 2011.

[57] J. Krantz *et al.*, "Spray-coated silver nanowires as top electrode layer in semitransparent P3HT:PCBM-based organic solar cell devices," *Adv. Funct. Mater.*, vol. 23, no. 13, pp. 1711–1717, 2013.

[58] J. Y. Lee, S. T. Connor, Y. Cui, and P. Peumans, "Semitransparent organic photovoltaic cells with laminated top electrode," *Nano Lett.*, vol. 10, no. 4, pp. 1276–1279, 2010.

[59] S. Coskun, E. S. Ates, and H. E. Unalan, "Optimization of silver nanowire networks for polymer light emitting diode electrodes," *Nanotechnology,* vol. 24, 2013.

[60] D. Raoufi and F. Hosseinpanahi, "The effect of film thickness on surface morphology of ITO thin films," *J. Theor. Appl. Phys.*, vol. 7, no. 1, p. 21, 2013.